



30 **Abstract**

31 Lake-land thermal contrasts significantly modulate regional air quality, yet the
32 coupling mechanisms which inland lakes regulate the diurnal evolution of $PM_{2.5}$ and its
33 components remain poorly understood. This study conducts high-resolution (1 km)
34 WRF-Chem simulations over Lake Chaohu and the adjacent megacity of Hefei, China,
35 to elucidate these interactions. Results reveal a distinct diurnal reversal effect. During
36 daytime, the lake presence facilitates a $PM_{2.5}$ increase exceeding $10 \mu\text{g}/\text{m}^3$ both over
37 the lake and in surrounding urban areas by suppressed planetary boundary layer height,
38 weakened vertical mixing, and reduced dry deposition velocities, which collectively
39 transform the lake into a “storage zone” that prolongs $PM_{2.5}$ lifetimes. This
40 accumulation is dominated by secondary $PM_{2.5}$, as the cooler and more humid lake air
41 thermodynamically favors the ammonium nitrate formation. Furthermore, convergence
42 zones where lake breezes meet background winds create localized stagnation traps that
43 intensify shoreline pollution. At night, while the lake surface maintains higher $PM_{2.5}$
44 concentrations than surrounding land, its impact on the city reverses, exerting a
45 purification effect with urban $PM_{2.5}$ decreasing by over $10 \mu\text{g}/\text{m}^3$ as land-breeze
46 circulation enhances vertical mixing and facilitates primary pollutant dispersion.
47 Sensitivity experiments reveal that failing to distinguish lake surfaces in emission
48 inventories can significantly amplify daytime pollution. These findings emphasize that
49 lakes act as complex dual regulators of urban air quality, with the identified mechanisms
50 likely applicable to other urban-lake systems globally. This study highlights the
51 necessity of high-resolution meteorological modeling and precise surface
52 characterization for improved air quality forecasting in lake-adjacent megacities
53 regions.

54

55

56

57



58 **1. Introduction**

59 Rapid urbanization and economic development in China over recent decades
60 have led to severe urban air pollution (e.g., Lei et al., 2011; Li et al., 2011; Liu et al.,
61 2018). Fine particulate matter (PM), known as PM_{2.5} (particulate matter with
62 aerodynamic diameters less than 2.5 μm), is the primary air pollutant (e.g., Zhang et al.,
63 2012; Hu et al., 2014a; Chai et al., 2014; Wang et al., 2014; He et al., 2017; Lu et al.,
64 2017). Ambient PM_{2.5} poses significant health risks including lung cancer, ischemic
65 heart disease, and respiratory disorders (e.g., Hu et al., 2014b; Guo et al., 2017; Ho et
66 al., 2018; Yang et al., 2019; Chen and Hoek, 2020; Yue et al., 2021), while also affecting
67 visibility (Li et al., 2014), radiation budget (Steiner et al., 2013), atmospheric
68 circulation (Jiang et al., 2017), cloud properties (Unger et al., 2009), and regional
69 climates (Guo et al., 2016; Li et al., 2016; Li et al., 2017c). The formation and evolution
70 of urban PM_{2.5} are comprehensively influenced by source emissions, long-range
71 transport, chemical transformations, and meteorological conditions (Guo et al., 2014;
72 Huang et al., 2014; Zhang et al., 2015b; Zhang et al., 2013; Hu et al., 2014c; Miao et
73 al., 2017; Miao et al., 2013; Zhang et al., 2015a). Among these factors, local-scale
74 underlying surface characteristics, such as land use type and surface cover, exert crucial
75 influence on PM_{2.5} distributions by altering surface energy balance, water cycles, and
76 momentum exchange, which subsequently affects turbulent mixing, pollutant transport,
77 deposition, and chemical processes.

78 Lakes exert a significant “lake effect” on surrounding areas through their
79 distinctive physical properties. Their high heat capacity, low albedo, and substantial
80 moisture supply create thermal contrasts with surrounding terrestrial surfaces,
81 modifying local and regional weather and climate patterns (Levy et al., 2010; Hayden
82 et al., 2011; Wentworth et al., 2015). Differential heating drives the formation of local
83 circulation systems. During daytime, solar heating warms land surfaces while
84 minimally affecting water, creating temperature gradients that generate pressure
85 gradients and initiate lake breezes (Atkinson, 1981; Stull, 1988). Air above the lake
86 moves inland in a shallow inflow layer while air aloft over land returns offshore. As



87 cooler lake air advances over warmer land surfaces, it forms a thermal internal
88 boundary layer (TIBL) that increases in height with inland distance (Lyons and Olsson,
89 1973; Garratt, 1990). At the leading edge of the lake breeze, air is forced upward at the
90 convergence zone (lake-breeze front) where cooler lake air meets warmer inland air,
91 producing enhanced vertical motion, increased moisture and wind shear, decreased
92 temperature, and directional wind shifts (Lyons, 1972). At night, the temperature
93 gradient reverses, generating a land breeze.

94 Lakes can significantly impact the atmospheric environment. Research on lake-
95 induced local circulation has been extensively conducted worldwide, predominantly
96 focusing on lake effects on ozone formation and distribution. Nocturnal stable boundary
97 layers and land breezes cause substantial accumulation of ozone and its precursors over
98 lake surfaces, resulting in significant ozone concentration increases after sunrise (Capps
99 et al., 2010; Fast and Heilman, 2005). Dye et al. (1995) demonstrated that temperature
100 inversions over Lake Michigan confine urban pollution over the lake, where other
101 emissions may be located within or above this inversion layer but experience limited
102 vertical mixing. Additionally, lake breezes transport ozone downwind during daytime.
103 Ozone moves landward via airflow and disperses upward under the influence of
104 updrafts at the lake breeze front (Lyons et al., 1995; Wentworth et al., 2015). Due to
105 downdrafts from the backflow effect, high ozone concentrations can be detected in mid-
106 lake regions (Burley et al., 2015; Hayden et al., 2011). Some pollutants may re-enter
107 the onshore airflow and spiral along the lake shoreline (Makar et al., 2010; Harris and
108 Kotamarthi, 2005). Levy et al. (2010) observed high O₃ concentrations over the
109 southern Great Lakes, where daytime updrafts transport O₃ to higher altitudes over
110 urban areas, while downdrafts subsequently transport O₃ back to the lake surface.
111 Furthermore, lake-breeze circulations can influence pollution transport by trapping
112 pollutants within the shallow TIBL (Sills et al., 2011), and the complex wind patterns
113 induced by lakes can cause rapid spatial variations in pollutant concentrations over
114 small distances (Hayden et al., 2011; Levy et al., 2008). Wang et al. (2023) found ozone
115 concentration in lakeshore areas within 5 km of Lake Taihu approximately 20 ppb
116 higher than other regions due to TIBL formation and lake-breeze regulation.



117 In addition to generating local circulation through thermal differences between
118 lakes and land surfaces, lakes also influence O₃ concentrations through modifications
119 to other critical meteorological conditions. Lakes can reduce air temperature and
120 planetary boundary layer height (PBLH) (Wang et al., 2017; Zhang et al., 2017) while
121 altering the spatial distribution of pollutant precursors (Hu and Xue, 2016; Li et al.,
122 2019), affecting both the diffusion of air pollutants and reaction conditions for
123 secondary pollutant formation, potentially causing ozone pollution in surrounding
124 urban areas. Furthermore, dry deposition rates of O₃ over water surfaces are
125 substantially lower compared to terrestrial surfaces (Monks et al., 2015), allowing O₃
126 to accumulate within the shallow boundary layer above the lake surface (Brook et al.,
127 2013). This reduced deposition efficiency contributes to the persistence and buildup of
128 ozone concentrations over lake areas, which can subsequently be transported to
129 adjacent regions through lake-breeze circulation patterns.

130 In contrast to the extensive literature on ozone, limited research has examined the
131 complex influence of lake effects on PM_{2.5}. Existing studies have primarily identified
132 that the vertical and horizontal motions within lake breeze circulation systems cause
133 the re-circulation of primary and secondary pollutants (Brook et al., 2013; Harris and
134 Kotamarthi, 2005) and enhance aerosol formation rates compared to the background
135 conditions (Brook et al., 2013; Hayden et al., 2011). For instance, increased
136 concentrations of secondary pollutants, such as sulfate and nitrate, have been observed
137 following lake breeze circulation events (Fosco and Schmeling, 2006). Despite these
138 findings, significant knowledge gaps remain. Existing studies have primarily focused
139 on individual processes or specific pollution episodes, lacking systematic investigation
140 into how lakes affect the spatial distribution and diurnal variation of PM_{2.5} and its
141 different components. Furthermore, the complex interactions among lake-related
142 processes, including local circulation, boundary layer mixing, dry deposition, and
143 chemical transformation, and how these processes collectively shape PM_{2.5} distribution
144 remain poorly understood. Moreover, existing research has been largely concentrated
145 in the North American Great Lakes region, while lake-urban interactions in rapidly
146 urbanizing areas characterized by intensive anthropogenic emissions, particularly in



147 East Asia, remain underexplored.

148 In summary, these research gaps highlight the need for systematic investigation
149 of lake effects on PM_{2.5} pollution. Existing studies lack systematic investigation into
150 how lakes affect the spatial distribution and diurnal variation of PM_{2.5} and its
151 components (primary and secondary aerosols) within lake-urban systems. Moreover,
152 how lake-related processes such as local circulation, boundary layer mixing, dry
153 deposition, and chemical transformation interact and collectively influence pollutant
154 concentrations remains poorly understood (Hayden et al., 2011; Zhang et al., 2017;
155 Wang et al., 2023). Lake Chaohu, one of China's five major freshwater lakes, provides
156 an ideal case for addressing these gaps. The megacity of Hefei, adjacent to the lake's
157 northern shore, forms a typical lake-urban system exemplifying the common global
158 pattern where large cities border natural water bodies (Chen et al., 2017; Peng et al.,
159 2019; Hu and Li, 2020). Rapid industrialization and urbanization in this region have
160 led to severe air pollution, yet the complex interactions between substantial urban
161 emissions and lake-induced meteorological effects remain underexplored. Therefore,
162 this study conducts high-resolution (1 km) WRF-Chem simulations with comparative
163 scenarios including (Lake) and excluding (Nolake) the lake to systematically
164 investigate how lake effects influence the spatiotemporal distribution of PM_{2.5} and its
165 key components, and to elucidate the coupling mechanisms between physical processes
166 (turbulent mixing, dry deposition, local circulation) and chemical processes. The
167 findings will provide scientific support for air quality forecasting and pollution control
168 strategies in lake-adjacent cities.

169 The paper is organized as follows: Section 2 introduces the WRF-Chem model
170 configuration, the design of different experiments, and emissions from different sources.
171 Section 3 presents the spatial distribution and diurnal variation of PM_{2.5} concentrations
172 from different sensitivity experiments and reveals the key mechanisms of lake effect on
173 the PM_{2.5}. Section 4 present the conclusion and discussion of the analysis.

174

175 **2. Methodology**



176 2.1 WRF-Chem

177 In this study, the version of WRF-Chem updated by the University of Science
178 and Technology of China (USTC version of WRF-Chem) is used. Compared with the
179 publicly released version, this USTC version of WRF-Chem includes some additional
180 functions such as the diagnosis of radiative forcing of aerosol species, land surface
181 coupled biogenic VOC (volatile organic compound) emission, aerosol-snow interaction,
182 improved PBL mixing of aerosols, and a detailed diagnosis of the contributions of each
183 crucial process to pollutant concentrations (Zhao et al., 2013a; Zhao et al., 2013b; Zhao
184 et al., 2014; Zhao et al., 2016; Hu et al., 2019; Du et al., 2020; Zhang et al., 2021; Yang
185 et al., 2025).

186 The configuration of WRF-Chem in this study is given in Table 1. In summary,
187 the Model for Simulating Aerosol Interactions and Chemistry (MOSAIC) and the
188 CBM-Z (carbon bond mechanism) photochemical mechanism (Zaveri and Peters, 1999)
189 are used. The MOSAIC aerosol scheme includes important physical and chemical
190 processes such as nucleation, condensation, coagulation, aqueous-phase chemistry, and
191 water uptake by aerosols. Sulfate (SO_4^{2-}), nitrate, (NO_3^-), ammonium (NH_4^+), sea salt,
192 mineral dust, organic matter (OM), black carbon (BC), and other (unspecified)
193 inorganics (OIN) constitute the prognostic species in MOSAIC. OIN represents the
194 unidentified aerosol species other than OM, BC, sulfate, ammonium, and nitrate in
195 emissions if any, which are composed mostly of minerals in emissions in this study.
196 The aerosol direct effect is coupled to the Rapid Radiative Transfer Model (RRTMG)
197 (Mlawer et al., 1997; Iacono et al., 2000) for both SW (shortwave) and LW (longwave)
198 radiation as implemented by Zhao et al. (2011). The optical properties and direct
199 radiative forcing of individual aerosol species in the atmosphere are diagnosed
200 following the methodology described in Zhao et al. (2013b). We also turned on the
201 aerosol indirect effect, which represents the interactions between aerosols and clouds,
202 including the first and second indirect effects, activation/resuspension, wet scavenging,
203 and aqueous chemistry (Gustafson et al., 2007; Chapman et al., 2009). The photolysis
204 rate is computed by the Fast-J radiation parameterization (Wild et al., 2000). Dry
205 deposition of aerosol mass and number is simulated following the approach of



206 Binkowski and Shankar (1995), which includes both particle diffusion and gravitational
207 effects. Another type of option include the Yonsei University (YSU) nonlocal PBL
208 parameterization scheme (Hong et al., 2006), the Noah land surface model (Chen and
209 Dudhia, 2001) for the surface layer process, and the Morrison two-moment scheme
210 (Morrison et al., 2009) for cloud microphysics.

211

212 **2.2 Numerical experiments**

213 The study period spans from 5 to 20 March 2019. Following previous research
214 (Yang et al., 2025), the first 5 day are considered to be the model spin-up time, while
215 the remaining integration period is used for analysis. Consequently, only the results
216 from 10 to 20 March 2019 are used in the analysis of this study. As shown in Figure 1a,
217 a three-domain nested simulation is implemented with spatial resolutions of 25, 5, and
218 1 km resolution, respectively. The outermost domain encompasses East, North, and
219 South China with 140 x 105 grid cells (107°-128°E, 17°-45°N) at 25 km horizontal
220 resolution. The intermediate domain covers the entire YRD region in East China,
221 consisting of 250 x 250 grid cells (111.8°-121.8°E, 27°-37°N) at 5 km resolution. The
222 innermost domain centers on Hefei City and encompasses Chaohu Lake, covering 150
223 x 150 grid cells (116.6°-117.8°E, 31.2°-32.4°N) at 1 km horizontal resolution. Domain
224 3 was selected as the main scope of study for this research, as shown in Figure 1b. Hefei,
225 the capital city of Anhui province and a typical megacity in the YRD, is located in the
226 mid-latitude zone with a humid subtropical monsoon climate. Chaohu Lake (31.40°-
227 31.72°N, 117.27°-117.85°E), China's fifth-largest freshwater lake, is situated in central
228 Anhui Province, approximately 15 km southeast of Hefei. The lake encompasses
229 approximately 780 km² with an average depth of 3 m and a 176 km shoreline. Thus, in
230 this study, the lake is characterized as a large, shallow, freshwater body situated within
231 an inland monsoon region, a configuration representative of numerous lakes in East
232 Asia. We define lake impact as the aggregate atmospheric perturbation driven by the
233 thermal and physical contrasts between the water surface and the surrounding terrestrial
234 landscape. This includes the modification of the surface energy balance, alterations in
235 aerodynamic roughness, and the regulation of atmospheric moisture, which collectively



236 govern the development of the internal boundary layer and the thermodynamic stability
237 of the overlying air. Specifically, this is expressed as the difference between the Lake
238 (control) and Nolake (sensitivity) experiments, or between the Lake_emis (control) and
239 Nolake_emis (sensitivity) experiments, as discussed below. This approach allows us to
240 isolate the net effect of the intrinsic physical and chemical properties of the lake on the
241 overlying atmosphere, providing a clear mathematical framework to evaluate how the
242 presence of the water body modulates the regional environment.

243 We derive terrain information from a high-resolution (~ 1 km) US Geological
244 Survey (USGS) topographic data and interpolate it onto the WRF grid. Furthermore, to
245 better resolve the PBL structure and mixing processes, we implemented a finer vertical
246 resolution within the PBL. A total of 50 terrain-following vertical eta-layers extending
247 from the surface to approximately 15 km were used, with 30 layers distributed below 2
248 km above the ground to describe the atmospheric boundary structure in detail. The
249 vertical layer was strategically designed with 7 layers below 200 meters (each
250 approximately 20 meters in height), 3 layers between 200 and 300 meters (each about
251 30 meters in height), and 8 layers between 300 and 1000 meters (each approximately
252 80 meters in height). This configuration comprehensively captures mixed layer
253 development and key turbulent processes (e.g., entrainment and surface flux exchange)
254 through layer densification, which is sufficient to capture PBL turbulent mixing.

255 Additionally, to ensure consistent boundary forcing across the three nested
256 domains, initial and boundary conditions are configured hierarchically. For the 25 km
257 resolution domain, meteorological initial and lateral boundary conditions are obtained
258 from the National Center for Environmental Prediction (NCEP) Final Reanalysis (FNL)
259 data at 1° x 1° resolution and 6 h temporal intervals. Initial and boundary conditions for
260 the trace gases and aerosol species are provided by the quasi-global WRF-Chem
261 simulation with 360 x 145 grid cells (67.5°S-77.5°N, 180°W-180°E) at 1° x 1°
262 resolution. The 5 km resolution simulation obtains its initial and boundary conditions
263 from the 25 km simulation output, while the 1 km resolution simulation is similarly
264 driven by the 5 km simulation results. Furthermore, the 25 km resolution simulation
265 turns on the option of cumulus parameterization, which uses the Kain-Fritsch cumulus



266 and shallow convection scheme (Kain, 2004) to simulate sub-grid scale clouds and
267 precipitation. However, this option is turned off in the other two higher-resolution
268 simulations because the fine-resolution is sufficient to resolve the cloud-forming
269 processes.

270 The land cover dataset is derived from a 1 km horizontal resolution dataset for
271 China (Zhang et al., 2021). The land use categories follow the United States Geological
272 Survey's (USGS) 24-category classification, and the dataset is based on China's land
273 cover conditions as of 2015. This provides a more accurate representation of current
274 land cover, particularly for eastern China, which has experienced intensive urban
275 expansion since the 2000s. Figure 2a shows the land cover data at 1 km resolution, with
276 detailed descriptions of the legend and land cover classes provided in Table S1 in the
277 Supplement. This set of simulations is referred to as the "Lake experiment". To evaluate
278 the impact of lake effects on meteorological conditions and PM_{2.5} concentrations in
279 surrounding urban regions, we conducted a sensitivity experiment in which Chaohu
280 Lake was replaced with cropland, the dominant land use type surrounding the lake, as
281 illustrated in Figure 2b. This experiment is referred to as the "Nolake experiment".
282 Specifically, only the lake area was replaced with cropland while preserving land-use
283 types in other regions, with all other conditions remaining unchanged, including initial
284 and boundary conditions, emissions, and parameterization schemes. With the exception
285 of part of Section 3.3, all other analyses in this study are based on the results of these
286 two comparative experiments.

287

288 **2.3 Emissions**

289 Conventionally, lake surfaces are regarded as emission-free areas, with
290 theoretical emission rates assumed to be zero. However, due to the coarse spatial
291 resolution of current emission inventories, most datasets cannot effectively distinguish
292 between land and lake surfaces. When emission inventories are spatially allocated or
293 downscaled to finer grid resolutions for air quality modeling, the lack of explicit lake-
294 land differentiation in these inventories results in emission fluxes being distributed
295 uniformly across grid cells, thereby erroneously assigning anthropogenic emissions to



296 lake areas that should theoretically be emission-free. Consequently, anthropogenic
297 emissions are often assigned to lake regions in many previous studies, which may
298 introduce biases and limit our understanding of atmospheric processes over lake
299 environments. To address the differences between scenarios with and without actual
300 emissions over the lake surface, this study designed four sets of comparative
301 experiments. The first two experiments are the previously mentioned “Lake experiment”
302 and “Nolake experiment”, in which lake surface emissions were masked (i.e., set to
303 zero), allowing investigation of how an emission-free lake surface affects the
304 distribution of particulate matter in the lake region and adjacent urban areas. The results
305 presented in Sections 3.1 and 3.2 are based on these two experiments. Additionally, to
306 assess scenarios where emissions are retained over the lake surface, a prevalent
307 configuration in current air quality modeling studies due to emission inventory
308 limitations, two additional experiments, “Lake_emis experiment” and “Nolake_emis
309 experiment”, were conducted. These experiments preserve the original lake emissions
310 while all other model settings remain consistent with the “Lake experiment” and
311 “Nolake experiment”. The purpose of these additional experiments is to evaluate how
312 the erroneous assignment of emissions to lake surfaces, a systematic bias resulting from
313 insufficient spatial resolution in emission inventories, may alter the lake effects
314 revealed in the idealized zero-emission scenarios and subsequently impact PM_{2.5}
315 distribution patterns in surrounding urban areas. Related analyses are presented in
316 Section 3.3. This four comprehensive experimental design enables systematic
317 evaluation of how both the presence of lake surfaces and the configuration of lake
318 emissions influence regional air pollution and lake-urban interactions.

319 For all simulations, anthropogenic emissions for the outer quasi-global
320 simulation are derived from the Hemispheric Transport of Air Pollution version-2
321 (HTAPv2) at 0.1° x 0.1° horizontal resolution with monthly temporal resolution for
322 2010 (Janssens-Maenhout et al., 2015). The Multi-resolution Emission Inventory for
323 China (MEIC) at 0.25° x 0.25° horizontal resolution for 2019 (Li et al., 2017a; Li et al.,
324 2017b; Zheng et al., 2018; Geng et al., 2024) is used to replace emissions over China
325 within the simulation domain. Specially, anthropogenic emissions for Domain 1 (D1)



326 are obtained from the original HTAPv2 and MEIC inventory interpolated to 25 km
327 resolution. Emissions for Domain 2 (D2) and Domain 3 (D3) are subsequently derived
328 by interpolating the 25 km resolution emissions to 5 km and 1 km resolution domains,
329 respectively. This study primarily focuses on PM_{2.5}. The spatial distribution of PM_{2.5}
330 emissions averaged over the entire day for both the Lake and Nolake experiments is
331 shown in Figure 2c, and Figure S1 illustrates the corresponding spatial distribution of
332 PM_{2.5} emissions in both the experiments at 08:00, 11:00, 14:00, 17:00, 20:00, 23:00,
333 02:00, and 05:00 local time (LT) throughout the study area. Additionally, the spatial
334 distribution of PM_{2.5} emissions in both the Lake_emis and Nolake_emis experiments
335 averaged over the entire day is shown in Figure S2. Biomass burning emissions are
336 obtained from the Fire Inventory from NCAR (FINN) at a 1 km horizontal resolution
337 and 1 h temporal resolution (Wiedinmyer et al., 2011). The diurnal variation in biomass-
338 burning emissions follows the suggestions by WRAP (2005), with injection heights
339 based on Dentener et al. (2006) from the Aerosol Comparison between Observations
340 and Models (AeroCom) project. Biogenic emissions were calculated using the Model
341 of Emissions of Gases and Aerosols from Nature (MEGAN) v3.0 model (Gustafson et
342 al., 2007; Zhang et al., 2021).

343

344 **3. Results**

345 **3.1 PM_{2.5} surface concentrations over lake and urban areas during daytime and** 346 **nighttime**

347 3.1.1 Diurnal reversal of lake effects on surface PM_{2.5} concentrations

348 The spatial distribution of PM_{2.5} surface concentrations in the Lake experiment
349 and the differences between the Lake and Nolake experiments at 08:00, 14:00, 20:00,
350 and 02:00 LT is illustrated in Figure 3. At 08:00 LT (Figure 3a), significant PM_{2.5}
351 pollution centers appeared in urban areas where concentrations typically exceeded 70
352 $\mu\text{g}/\text{m}^3$, while lake area concentrations in the Lake experiment reached 50-60 $\mu\text{g}/\text{m}^3$.
353 Figure 3b presents that PM_{2.5} concentrations over the lake region in the Lake
354 experiment significantly exceeded those in the Nolake experiment by more than 15



355 $\mu\text{g}/\text{m}^3$. Additionally, the lake presence induced varying degrees of $\text{PM}_{2.5}$ concentration
356 enhancement in urban areas to the north and northwest. These results indicate that the
357 lake enhances pollutant accumulation over its surface and facilitates transport to
358 surrounding regions through atmospheric dispersion, thereby exacerbating urban $\text{PM}_{2.5}$
359 pollution during morning. At 14:00 LT, $\text{PM}_{2.5}$ concentrations throughout the region
360 decreased substantially (Figure 3c), with urban concentrations declining to
361 approximately 30–40 $\mu\text{g}/\text{m}^3$ due to daytime boundary layer development and enhanced
362 dispersion. Over the lake area, $\text{PM}_{2.5}$ concentrations in the Lake experiment approached
363 40 $\mu\text{g}/\text{m}^3$, comparable to urban concentrations and substantially higher than
364 corresponding values in the Nolake experiment. The difference shown in Figure 3d
365 reveals that the lake's pollution-enhancing effect peaked during afternoon. Specifically,
366 $\text{PM}_{2.5}$ concentrations in the Lake experiment over the lake surface significantly
367 exceeded those in the Nolake experiment by more than 10 $\mu\text{g}/\text{m}^3$. Compared to 8:00 LT,
368 pollutant dispersion from the lake surface to surrounding areas extended over greater
369 distances in the Lake experiment, with more pronounced relative differences in
370 concentrations. Significant concentration enhancement zones approximately 10 $\mu\text{g}/\text{m}^3$
371 forming around the lake perimeter. These results indicate that the lake's pollution-
372 enhancing effect intensifies during afternoon and further exacerbates air pollution in
373 surrounding urban areas.

374 Additionally, to validate the reasonableness of simulated $\text{PM}_{2.5}$ concentrations
375 over the lake, this study compared results with the satellite-derived hourly 5 km (i.e.,
376 H5K) ground-level $\text{PM}_{2.5}$ dataset for Eastern China (ChinaHigh $\text{PM}_{2.5}$) (Wei et al., 2021),
377 which provides hourly surface $\text{PM}_{2.5}$ concentrations during 08:00-17:00 LT. Figure S4
378 shows that $\text{PM}_{2.5}$ concentrations over the lake are comparable to or exceed those in
379 surrounding urban areas during daytime, particularly during 11:00-16:00 LT (Figure
380 S4d-i). These observations validate the daytime pollutant accumulation over the lake
381 surface discovered in our Lake experiment.

382 During nighttime, the lake impact on surrounding air quality underwent a
383 fundamental reversal. At 20:00 LT, regional $\text{PM}_{2.5}$ concentrations increased rapidly due
384 to reduced nighttime PBLH and deteriorated dispersion conditions, as shown in Figure



385 3e. In urban areas, $PM_{2.5}$ concentrations in the Lake experiment exceeded $80 \mu\text{g}/\text{m}^3$,
386 while concentrations over the lake surface ranged from approximately $40\text{--}50 \mu\text{g}/\text{m}^3$.
387 Figure 3f clearly demonstrates that $PM_{2.5}$ concentrations over the lake surface in the
388 Lake experiment remained higher than those in the Nolake experiment by more than 10
389 $\mu\text{g}/\text{m}^3$, consistent with daytime patterns. However, the lake presence significantly
390 reduced $PM_{2.5}$ concentrations in urban areas to its north and northwest, with reductions
391 generally exceeding $10 \mu\text{g}/\text{m}^3$. This phenomenon indicates that the lake exerted a
392 distinct and continuous purification effect on surrounding urban areas during nighttime.
393 By 2:00 LT, high-concentration pollution masses continued to persist and accumulate
394 in urban areas, with concentrations in the central urban area exceeding $90 \mu\text{g}/\text{m}^3$ (Figure
395 3g). The lake area maintained higher concentrations in the Lake experiment compared
396 to the Nolake experiment (Figure 3h). The nighttime purification effect persisted at
397 02:00 LT, with $PM_{2.5}$ concentrations in the Lake experiment remaining lower in urban
398 areas by $0\text{--}15 \mu\text{g}/\text{m}^3$. Although the spatial extent and pattern of the purification effect
399 evolved slightly compared to 20:00 LT, the improvement effect of the lake on urban air
400 quality remained stable and persistent throughout the night. The spatial distributions of
401 $PM_{2.5}$ surface concentrations in the Lake and Nolake experiments at 11:00, 17:00, 23:00,
402 and 05:00 LT displayed patterns consistent with those at 08:00, 14:00, 20:00, and 02:00
403 LT (Fig. S3), further validating the stability and reproducibility of the diurnal variation
404 in the lake's impact on local $PM_{2.5}$ concentrations. The lake exhibits significant diurnal
405 variation in its influence on local $PM_{2.5}$ concentrations, consistently maintaining higher
406 concentrations over the lake surface than in the Nolake experiment. The lake's impact
407 on surrounding urban areas shows distinct diurnal differences, enhancing urban $PM_{2.5}$
408 concentrations by up to $15 \mu\text{g}/\text{m}^3$ during daytime with peak effects at 14:00 LT, while
409 reducing concentrations by approximately $10 \mu\text{g}/\text{m}^3$ during nighttime, revealing a dual
410 role in regulating local air quality.

411 Furthermore, to more clearly quantify the $PM_{2.5}$ concentration differences
412 between the Lake and Nolake experiments and their temporal and spatial variations,
413 Figure 4 presents the diurnal variation of $PM_{2.5}$ concentrations along the key path
414 indicated in Figure 3. Figure 4a compares the average $PM_{2.5}$ concentration differences



415 along this transect during daytime (the average of 08:00, 11:00, 14:00, and 17:00) and
416 nighttime (the average of 20:00, 23:00, 02:00, and 05:00). During daytime, the presence
417 of the lake consistently elevates $PM_{2.5}$ concentrations along the transect, with the most
418 significant impact at point B adjacent to the lakeshore (0 km distance), where the peak
419 difference exceeds $8 \mu\text{g}/\text{m}^3$. This effect gradually weakens with increasing distance and
420 stabilizes at $0\text{-}2 \mu\text{g}/\text{m}^3$ beyond approximately 15 kilometers. At night, a significant
421 purification effect is observed. At point B, the concentration difference is slightly
422 positive but rapidly becomes negative approximately 3 kilometers from the lakeshore,
423 reaching maximum purification effectiveness in the urban center 16-17 kilometers from
424 point B, with concentration reductions approaching $8 \mu\text{g}/\text{m}^3$. This indicates that the
425 most significant nighttime purification occurs not immediately adjacent to the lakeshore
426 but rather appears in areas at a certain distance from the lakeshore.

427 Figures 4b shows the evolution of $PM_{2.5}$ concentrations along the path with time
428 and distance for the Lake experiments, exhibiting strong diurnal variation. During
429 nighttime to early morning (approximately 19:00–08:00 LT), $PM_{2.5}$ concentrations
430 exceed $70 \mu\text{g}/\text{m}^3$ due to persistent pollutant accumulation under stable boundary layer
431 conditions. During daytime (approximately 09:00–18:00 LT), concentrations decrease
432 significantly to $30\text{-}50 \mu\text{g}/\text{m}^3$ as the boundary layer develops and dispersion conditions
433 improve. Figure 4c displays the diurnal variation of $PM_{2.5}$ concentration differences
434 between the Lake and Nolake experiments with distance, revealing the day-night
435 reversal in the impact of the lake. During daytime, $PM_{2.5}$ concentrations are higher in
436 the Lake experiment, with the greatest enhancement occurring in the near-lake area 0-
437 6 kilometers from point B, where the maximum increase exceeds $8 \mu\text{g}/\text{m}^3$, decreasing
438 with increasing distance. Notably, the influence range is most extensive at 14:00 LT,
439 with concentration increases of $2\text{-}4 \mu\text{g}/\text{m}^3$ still present within 15 kilometers from the
440 lakeshore, consistent with the daytime performance shown in Figure 4a. At night, $PM_{2.5}$
441 concentrations decrease, with more significant reductions at certain distances from the
442 shore. For example, at 20:00 LT in the area approximately 12-18 kilometers from point
443 B, maximum reductions exceed $8 \mu\text{g}/\text{m}^3$. To further investigate the diurnal reversal
444 pattern at different times, Figure S5 shows the distribution of average $PM_{2.5}$



445 concentration differences along the path at eight key moments. The results are highly
446 consistent with Figure 4, revealing in greater detail the intensity variations, influence
447 ranges, and temporal evolution of the pollution enhancement and purification effects.
448 Overall, the lake exerts a strong diurnal regulatory effect on local PM_{2.5} concentrations,
449 exacerbating pollution in near-shore areas during daytime while providing a
450 purification effect for surrounding urban areas during nighttime.

451

452 3.1.2 Component-dependent response of PM_{2.5} to lake effects

453 Furthermore, PM_{2.5} is composed of different components, yet the diurnal
454 variation characteristics of these different components and their response mechanisms
455 to lake influence remain unclear. To investigate the different impact of the lake on
456 various PM_{2.5} components, this study conducted an in-depth analysis of primary and
457 secondary PM_{2.5}, as shown in Figures 5 and 6. During daytime, secondary PM_{2.5} plays
458 a particularly prominent role and dominates the concentration differences. At 14:00 LT
459 (Figures 5c, 5d, 6c and 6d), the increase of secondary PM_{2.5} concentration over the
460 lake is generally 5-10 µg/m³, which is not only significantly greater than the 0-5 µg/m³
461 increase in primary PM_{2.5}, but also extends over a broader range and degree of influence
462 in surrounding areas. Therefore, the differences between the Lake and Nolake
463 experiments in urban areas mainly stem from pollutant transport from the lake surface,
464 with secondary particles exerting a greater impact than primary particles. Notably,
465 secondary PM_{2.5} concentrations over the lake are 15-18 µg/m³, while secondary PM_{2.5}
466 concentrations in urban areas in the Lake experiment are approximately 12-15 µg/m³,
467 forming an anomalous pollution where lake surface concentrations exceed urban
468 concentrations, which differs dramatically from conventional understanding.
469 Ultimately, these secondary particles that abnormally accumulate over the lake surface
470 are subsequently transported to urban areas through physical processes such as lake-
471 breeze circulation and dispersion, becoming a key factor in exacerbating urban daytime
472 PM_{2.5} pollution.

473 During nighttime, however, the dominant mechanism undergoes a fundamental
474 reversal, with physical transport of primary PM_{2.5} becoming the key factor determining



475 changes in total $PM_{2.5}$ concentrations in urban areas. Primary $PM_{2.5}$ concentrations in
476 urban areas are substantially reduced due to the lake presence, while secondary $PM_{2.5}$
477 reductions are relatively limited. Therefore, primary $PM_{2.5}$ dominate the spatial
478 distribution of $PM_{2.5}$ concentrations in urban areas during nighttime. At 20:00 LT
479 (Figures 5f and 6f), widespread reductions in primary $PM_{2.5}$ concentrations occur across
480 urban areas, with decreases exceeding $10 \mu\text{g}/\text{m}^3$ that correspond closely to the negative
481 difference zones of total $PM_{2.5}$. In contrast, secondary $PM_{2.5}$ reductions are much
482 weaker, with scattered affected areas and intensities generally ranging between 0-3
483 $\mu\text{g}/\text{m}^3$, indicating that the nighttime purification effect is primarily achieved through
484 effective removal of directly emitted pollutants (primary $PM_{2.5}$). Additionally, Figures
485 S6 and S7 show the primary and secondary $PM_{2.5}$ distribution at several other time
486 points, with the overall pattern consistent with these results. In summary, the impact of
487 lake on $PM_{2.5}$ exhibits significant component-dependency and diurnal transition
488 characteristics. The nighttime purification effect is dominated by physical removal of
489 primary $PM_{2.5}$, while the daytime pollution enhancement effect, particularly the
490 formation of extreme concentrations above the lake, is closely related to the unique
491 chemical-physical interactions involving secondary $PM_{2.5}$.

492

493 **3.2 The influence mechanism of $PM_{2.5}$ concentrations over the lake and urban** 494 **areas**

495 To elucidate the fundamental physical and chemical mechanisms underlying the
496 diurnal reversal effect of lakes on $PM_{2.5}$ concentrations, we conducted an in-depth
497 analysis of the evolution of $PM_{2.5}$ and its associated physical, dynamic, and chemical
498 drivers in this section.

499

500 3.2.1 Spatiotemporal evolution of $PM_{2.5}$ vertical distribution

501 Figure 7 presents the vertical cross-section of $PM_{2.5}$ concentrations and wind
502 speed along the key path AC (as shown in Fig. 2). At 08:00, the $PM_{2.5}$ high-
503 concentration zone in both experiments was primarily concentrated below 0.3 km in
504 urban areas, exceeding $55 \mu\text{g}/\text{m}^3$, while concentrations over the lake region were



505 relatively low. The lake effect had already begun to manifest. Figure 7c shows near-
506 surface $PM_{2.5}$ concentrations over the lake were significantly higher in the Lake
507 experiment, with peak differences exceeding $5 \mu\text{g}/\text{m}^3$, spreading toward surrounding
508 urban areas and maintaining substantial differences at considerable distances from the
509 lakeshore. Notably, near the top of the boundary layer, $PM_{2.5}$ concentrations in the Lake
510 experiment were actually lower than those in the Nolake experiment. At 14:00,
511 although $PM_{2.5}$ concentrations generally decreased to $20\text{-}35 \mu\text{g}/\text{m}^3$ due to boundary
512 layer development, the pollution-enhancing effect of the lake peaked. The high-
513 concentration layer extending upward to approximately 1.5 km altitude with more
514 uniform vertical mixing. Figure 7f shows maximum positive concentration differences
515 of approximately $10 \mu\text{g}/\text{m}^3$ over the lake region, extending upward to nearly 1 km in
516 height. This effect significantly spread both horizontally and vertically toward adjacent
517 urban areas, forming an extensive strong positive difference zone in the lakeside region
518 that stretched from the near-surface up to 1.3 km altitude. Compared to 08:00, the
519 afternoon $PM_{2.5}$ concentration increase was larger with broader impact range, further
520 exacerbating air pollution in surrounding urban areas, consistent with the horizontal
521 distribution patterns described earlier.

522 At 20:00 and 02:00 LT (Figures 7g-l), decreased PBLH causes pollutants to re-
523 accumulate near the urban surface, forming a shallow pollution layer exceeding 55
524 $\mu\text{g}/\text{m}^3$. Over the lake area, $PM_{2.5}$ concentrations near the lake surface in the Lake
525 experiment remained higher than in the Nolake experiment, while concentrations above
526 the lake surface were lower. In urban areas, the nighttime differences exhibit
527 distribution characteristics completely opposite to daytime. The vertical cross-sections
528 (Figures 7i, l) reveal a “negative below, positive above” difference pattern. Near-surface
529 $PM_{2.5}$ concentrations are lower in the Lake experiment with maximum decreases of
530 approximately $15 \mu\text{g}/\text{m}^3$, while at higher boundary layer levels, the situation is
531 completely reversed, $PM_{2.5}$ concentrations are higher in the Lake experiment by
532 approximately $0\text{-}10 \mu\text{g}/\text{m}^3$. Other periods also exhibit the same vertical distribution, as
533 shown in Figures S8.

534



535 3.2.2 Lake-induced meteorological regulation and the accumulation of PM_{2.5} over the
536 lake

537 The unique physical properties of lakes constitute the intrinsic mechanism
538 underlying these concentration variations. First, the lake significantly suppresses
539 boundary layer development above its surface. As shown in Figure 7, the PBLH over
540 the lake surface in the Lake experiment is markedly lower than in the Nolake
541 experiment, particularly at 14:00 (Figure 7d), where it was suppressed to an extremely
542 shallow level of less than 0.1 km while the boundary layer in the Nolake experiment
543 had developed to nearly 1.5 km. This reduced PBLH inhibits the upward dispersion of
544 PM_{2.5} from the lake region, causing particles to accumulate over the lake surface and
545 thereby increasing PM_{2.5} concentrations. At 20:00 and 02:00 LT (Figures 7g-l), the
546 nighttime boundary layer height in the Lake experiment remained substantially lower
547 than in the Nolake experiment, strongly inhibiting upward PM_{2.5} diffusion above the
548 lake surface.

549 Second, the lake substantially weakens vertical mixing capacity above it. During
550 daytime, land areas exhibit strong mixing with generally high mixing coefficients,
551 particularly in urban areas where values exceed 15 m²/s, as shown in Figure 8a.
552 However, mixing capacity above the lake is significantly suppressed, with extremely
553 low mixing coefficients of approximately 0-0.4 m²/s. Figure 8b demonstrates that the
554 lake presence greatly reduced daytime boundary layer mixing intensity compared to the
555 Nolake experiment. During nighttime, the PBL mixing coefficient above the lake in the
556 Lake experiment remained over 40% lower than in the Nolake experiment (Figure 8d).
557 This weakened mixing stems from two primary mechanisms. First, the large specific
558 heat capacity of lake water causes slow daytime warming, resulting in surface
559 temperatures lower than those of surrounding land. This thermal contrast creates stable
560 atmospheric stratification that suppresses vertical thermal turbulence, leading to rapid
561 PM_{2.5} accumulation over the lake surface. Second, the significantly lower aerodynamic
562 roughness of the lake surface compared to land plays a crucial role. The smooth water
563 surface generates considerably less mechanical turbulence (wind shear) than the
564 rougher farmland surface in the Nolake experiment. Consequently, the lack of



565 mechanical mixing further inhibits vertical diffusion, maintaining the storage effect of
566 the lake.

567 Furthermore, dry deposition velocity differs significantly between the lake and
568 land surface. Figure 9 shows the spatial distribution of dry deposition velocity in the
569 study area. Daytime land areas, especially urban surfaces, exhibit relatively high dry
570 deposition velocity reaching up to 0.045 m/s. However, dry deposition velocity over
571 the lake in the Lake experiment was extremely low, approaching zero, while in the
572 Nolake experiment, the farmland surface replacement increased dry deposition velocity
573 dramatically to 0.025-0.03 m/s (Figure 9a). Figure 9b clearly shows that the lake
574 significantly reduced the dry deposition velocity in this region. During nighttime, the
575 lake also significantly reduced dry deposition velocity above its surface, with decreases
576 far exceeding 10% (Figure 9d). This indicates that the lake water body acts as an
577 extremely inefficient deposition surface, making it difficult for pollutants to settle on
578 its surface, directly leading to prolonged $PM_{2.5}$ lifetimes and more pronounced pollution
579 accumulation in the near-surface boundary layer.

580 Figure 10 further illustrates the spatial distribution of $PM_{2.5}$ lifetimes in the study
581 area. During daytime, land areas show relatively short $PM_{2.5}$ lifetimes, particularly in
582 urban areas where they are only 50-100 hours attributed to higher dry deposition rates
583 that promote pollutant removal. In the Lake experiment (Figure 10a), $PM_{2.5}$ lifetimes
584 over the lake surface exhibited extremely high values exceeding 1500 hours, forming a
585 stark contrast with surrounding land areas. Figure 10b shows that the lake presence
586 even increased $PM_{2.5}$ lifetimes above its surface by over 800 hours. During nighttime,
587 the lake similarly extended pollutant lifetimes (Figure 10d), with maximum increases
588 of approximately 500 hours. This demonstrates that the combined effects of the
589 compressed boundary layer, weak turbulent mixing, and significantly reduced dry
590 deposition velocity over the lake work synergistically to inhibit $PM_{2.5}$ removal in the
591 lake region, making the lake a “storage zone” for particles, thereby causing strong near-
592 surface pollutant accumulation.

593

594 3.2.3 Lake-induced transport regulation and the redistribution of $PM_{2.5}$ in urban areas



595 While physical mechanisms lead to pollutant accumulation, dynamic processes
596 drive the transport and redistribution of these particles. Over the lake area, near-surface
597 PM_{2.5} concentrations in the Lake experiment are substantially higher than in the Nolake
598 experiment due to suppressed boundary layer development, weakened turbulent mixing,
599 and reduced dry deposition velocity. However, this accumulation is largely confined to
600 the near-surface layer. At upper levels, the pattern reverses. The Nolake experiment
601 shows higher PM_{2.5} concentrations as stronger thermal turbulence from the farmland
602 surface mixes more pollutants to higher altitudes, whereas the Lake experiment
603 maintains a more stable atmosphere that suppresses vertical mixing. This mechanism
604 operates consistently during both daytime and nighttime, as validated by the vertical
605 profiles of PM_{2.5} concentrations in Figure S9. Figures S9b and S9d demonstrate that
606 over the lake area, PM_{2.5} concentrations in the Lake experiment remain higher near the
607 surface but lower aloft than in the Nolake experiment throughout the diurnal cycle. This
608 vertically-stratified pollution structure over the lake represents only the direct local
609 effect. The lake's influence extends to surrounding urban areas through complex
610 dynamical transport processes that redistribute these pollutants both horizontally and
611 vertically. These lake-induced perturbations to urban areas exhibit distinct mechanisms
612 during daytime (horizontal convergence and frontal stagnation) and nighttime
613 (enhanced vertical redistribution). These dual mechanisms govern the spatiotemporal
614 patterns of lake-urban PM_{2.5} interactions and explain the observed diurnal reversal
615 effect in urban air quality.

616 During daytime, this influence manifests primarily through horizontal transport
617 processes coupled with lake breeze-background wind interactions. High-pollution air
618 masses formed over the lake affect surrounding urban areas through horizontal transport
619 by concentration gradients between the lake and city. As PM_{2.5} concentrations over the
620 lake increase significantly, pollutants diffuse outward, creating a positive difference
621 layer extending from the lake to the city from the surface to nearly 1 km altitude, with
622 maximum concentration differences of approximately 10 µg/m³. The dramatic PM_{2.5}
623 increases in specific lakefront regions, particularly the southwestern shore, result from
624 intense dynamical interactions between lake breeze circulation and the background



625 wind field. At 14:00 LT, peak solar radiation creates maximum lake-land temperature
626 differences, driving lake breeze formation that radiates outward and superimposes on
627 the prevailing southwest wind (Figure 11d). In the southwestern lake region, the
628 northeastward lake breeze meets the background southwest wind head-on, forming a
629 persistent convergence line termed the “lake breeze front” that acts as a dynamical
630 barrier. This front creates a horizontal stagnation zone with sharply reduced wind
631 speeds (Figure 11f), trapping high-concentration pollutants diffusing from the lake and
632 those carried by the background wind, causing concentrations to spike. Figure S10
633 shows wind speed at other times, displaying varying degrees of daytime dynamical
634 convergence. Cross-sectional analysis along pathway AC (Figure 7d) further confirms
635 this mechanism, showing airflow from the urban area being strongly lifted by lake-area
636 airflow near the lakeshore, blocking background airflow advance and forcing strong
637 upward motion, a typical characteristic of convergence zones absent in the Nolake
638 experiment. At the northern shore, the southward lake breeze converges with the
639 westward background wind, creating less intense but still significant convergence. At
640 the northeastern shore, the lake breeze aligns with the background southwest wind,
641 preventing frontal convergence, so pollutant accumulation results solely from diffusion
642 with much smaller intensity. While lake-induced meteorological perturbations to urban
643 areas remain relatively limited during daytime due to vigorous urban boundary layer
644 development, intense turbulent mixing, and strong dry deposition velocity (Figures 8b
645 and 9b), the lake breeze-driven convergence mechanism creates localized “pollutant
646 stagnation traps” at strategic locations where opposing wind systems meet,
647 fundamentally altering pollution patterns along specific lakefront areas.

648 In stark contrast to the daytime horizontal convergence and gradient-driven
649 diffusion, nighttime dynamics are dominated by enhanced vertical redistribution that
650 reverses the lake’s effect on near-surface urban air quality. As shown in Figures 7i and
651 7l, the urban area exhibits a distinct “negative-below, positive-above” difference pattern
652 stemming from lake-induced perturbation effect. Figure 12 reveals the underlying
653 mechanism by showing the net contribution of vertical mixing to $PM_{2.5}$ concentrations
654 along path AC. In urban areas under both scenarios (Figures 12a, b), vertical mixing



655 presents a “negative below, positive above” contribution pattern. Near the surface,
656 pollutants are transported upward by turbulent mixing, leading to strong negative
657 contributions below $-16 \mu\text{g}/\text{m}^3$. Meanwhile, within the boundary layer above
658 (approximately below 0.3 km), strong positive contributions far exceeding $+16 \mu\text{g}/\text{m}^3$
659 occur due to pollutants reception from below. The difference between experiments
660 (Figure 12c) reveals that near the urban surface, negative difference values indicate
661 greater concentration reduction in the Lake experiment, while positive values aloft
662 indicate greater concentration increases, demonstrating that PBL vertical mixing
663 intensity in urban areas is much greater in the Lake experiment. The underlying
664 mechanism involves land breeze circulation driven by lake-land thermal contrasts,
665 which induces additional dynamic turbulence and upward motion above the city,
666 disrupting typical nighttime stable conditions. This lake-enhanced vertical mixing more
667 efficiently transports accumulated near-surface pollutants upward, achieving effective
668 purification of near-surface urban air. Figure S9c validates these results, showing lower
669 $\text{PM}_{2.5}$ concentrations near the urban surface but higher concentrations at 100-300 m
670 altitude in the Lake experiment during nighttime, indicating a dynamic process
671 transporting near-surface pollutants upward driven by lake-induced perturbations to
672 urban meteorological fields and PBL vertical mixing processes.

673

674 3.2.4 Lake-induced chemical regulation and the formation of secondary $\text{PM}_{2.5}$

675 Beyond the physical and dynamical mechanisms discussed above, lakes
676 profoundly influence $\text{PM}_{2.5}$ distributions by regulating atmospheric chemical processes,
677 particularly for secondary aerosols. As revealed in Section 3.1.2, secondary $\text{PM}_{2.5}$
678 concentration differences between the Lake and Nolake experiments over the lake
679 region at 14:00 significantly exceed those of primary $\text{PM}_{2.5}$, with lake surface
680 concentrations reaching or exceeding urban levels. This stems from fundamental
681 differences in formation mechanisms and thermodynamic sensitivity. While primary
682 $\text{PM}_{2.5}$ (BC, OC, OIN) originates mainly from direct emissions with minimal chemical
683 transformations, secondary $\text{PM}_{2.5}$ formation is highly sensitive to temperature and
684 humidity, which lakes powerfully regulate through their large heat capacity. The



685 ammonium nitrate formation process ($\text{NH}_3 + \text{HNO}_3 \rightleftharpoons \text{NH}_4\text{NO}_3$) exhibits
686 thermodynamic reversibility, which decreased temperature or increased humidity
687 promotes particulate NH_4NO_3 formation, while high-temperature and low-humidity
688 cause decomposition into NH_3 and HNO_3 gases. In contrast, sulfate formation through
689 SO_2 oxidation is almost irreversible and demonstrates greater atmospheric stability.

690 At 08:00, chemical contributions remain consistent between experiments,
691 showing weak net production ($6\text{-}10 \mu\text{g}/\text{m}^3$) in near-surface urban areas due to precursor
692 enrichment from traffic, industrial, and domestic activities, while lake contributions
693 approach zero (Figure S11a, c). At 14:00, however, dramatically different patterns
694 emerge (Figures S11b and S11d). In the Nolake experiment, elevated temperatures and
695 lower humidity below 0.5 km promote NH_4NO_3 decomposition, producing strong
696 negative $\text{PM}_{2.5}$ contributions (exceeding $-16 \mu\text{g}/\text{m}^3$), while turbulent transport carries
697 decomposed precursors to 0.5-1.5 km altitudes where lower temperatures and higher
698 humidity favor re-condensation, creating strong positive contributions (exceeding 16
699 $\mu\text{g}/\text{m}^3$). Conversely, the Lake experiment shows near-zero chemical contributions
700 throughout the lake area from surface to upper atmosphere. Higher humidity and slower
701 temperature increases due to large heat capacity enhance NH_4NO_3 stability and
702 suppress decomposition, reducing near-surface decomposition, cutting off precursor
703 transport to higher altitudes, and minimizing chemical influence due to weak vertical
704 transport and mixing. These combined effects result maximum nitrate and ammonium
705 concentration differences between experiments at 14:00, with nitrates and ammonium
706 passively accumulating over the lake exceeding urban concentrations (Figures S12 and
707 S13). In comparison, sulfate differences remain much smaller (Figure S14) due to
708 sulfate's irreversible formation and atmospheric stability. In summary, lakes impact
709 secondary $\text{PM}_{2.5}$ during daytime more than primary $\text{PM}_{2.5}$ by regulating local
710 temperature and humidity, profoundly intervening in reversible chemical equilibria and
711 transforming themselves from passive surface types into efficient pollutant “storage
712 zones.”

713

714 **3.3 $\text{PM}_{2.5}$ surface concentrations over lake and urban areas during daytime and**



715 **nighttime under artificial lake emission scenarios**

716 The preceding analysis systematically revealed the complex lake effect on PM_{2.5}
717 concentrations through meteorological field alterations under the idealized zero-
718 emission lake scenario. However, practical air quality modeling faces pervasive
719 uncertainty from limited emission inventory spatial resolution. Most current inventories
720 cannot effectively distinguish land from lake areas, erroneously assigning emissions to
721 lakes that should have none. This systematic bias may significantly alter lake effects.
722 To assess the real impact of such emission configuration on regional air pollution and
723 lake-urban interactions, we designed two additional control experiments (Lake_emis
724 and Nolake_emis) retaining original emission settings over lake surfaces, with all other
725 parameters consistent with previous two experiments (Lake and Nolake). Comparing
726 these experiments thoroughly investigates how lake surface emissions, prevalent in
727 current simulations, impact PM_{2.5} distribution in surrounding urban areas.

728 Figure 13 shows the spatial distribution of surface PM_{2.5} concentrations in the
729 Lake_emis experiment and differences between Lake_emis and Nolake_emis at 08:00,
730 14:00, 20:00, and 02:00 under the scenario retaining the original emission inventory
731 over lake surfaces. At 08:00 (Figures 13a-b), high pollution centers remain in urban
732 areas with concentrations exceeding 80 µg/m³ regardless of lake presence, with peak
733 concentration differences in the lake area exceeding 20 µg/m³. At 14:00 (Figures 13c-
734 d), the lake area becomes an extremely prominent pollution hotspot with concentrations
735 reaching 50-80 µg/m³, far exceeding urban concentrations of 35-40 µg/m³. Compared
736 to the scenario without lake emissions (Figure 3d), positive differences intensify
737 dramatically in the lake region with peak values approaching 60 µg/m³, while
738 surrounding areas also exhibit strong positive differences, indicating that direct daytime
739 lake emissions synergize with physical accumulation mechanisms to jointly exacerbate
740 pollution over the lake and surrounding urban areas. Figures S15a-d confirm this pattern
741 persists at 11:00 and 17:00. At 20:00 (Figures 13e-f), regional pollution rises again with
742 high concentrations centered in urban areas, while the lake region maintains strong
743 positive differences due to continuous emissions combined with weak nighttime
744 boundary layer mixing and low dry deposition. However, urban areas still exhibit



745 significant negative differences with maximum reductions are approximately $30 \mu\text{g}/\text{m}^3$,
746 demonstrating that the lake's physical purification mechanism for urban areas persists
747 even with lake surface emissions. At 02:00 (Figures 13g-h), urban pollution remains
748 elevated while concentration differences stay negative at approximately $-20 \mu\text{g}/\text{m}^3$,
749 further confirming the lake's significant nighttime purification effect. Notably, both
750 positive and negative differences coexist in the lake region, potentially reflecting
751 complex physicochemical mechanisms introduced by lake emissions. Figures S15e-h
752 at 23:00 and 05:00 confirm these phenomena.

753 Furthermore, Figure 14 shows the vertical cross-sections of $\text{PM}_{2.5}$ concentrations
754 along the AC pathway under the retained lake emission scenario, revealing how lake
755 emissions alter $\text{PM}_{2.5}$ vertical structure. During daytime, lake surface emissions
756 synergize with the lake's intrinsic physical properties, emerging at 08:00 and peaking
757 at 14:00. At 08:00 (Figures 14a-c), although high-concentration zones in both
758 experiments remain near the urban surface, differences already reveal significant
759 positive layers over the lake area. By 14:00 (Figures 14d-f), this difference amplifies
760 dramatically. While the Nolake_emis experiment confines high pollution to the deep
761 urban boundary layer, Lake_emis experiment transforms the lake into a new pollution
762 core with intensity far exceeding the city, with $\text{PM}_{2.5}$ hotspots exceeding $55 \mu\text{g}/\text{m}^3$
763 hovering over the lake. Differences (Figure 14f) show large positive areas exceeding
764 $40 \mu\text{g}/\text{m}^3$ covering the entire lake area and surroundings. Figures S16a-f confirm similar
765 distributions at 11:00 and 17:00, demonstrating that direct lake emissions synergize
766 with unique daytime physical accumulation mechanisms such as compressed boundary
767 layers and weak dry deposition, making the lake an anomalous pollution source
768 exceeding major urban sources. Nighttime cross-sections (Figures 14g-l) confirm that
769 even with lake emissions, the lake-driven physical purification mechanism significantly
770 effects urban areas through persistent negative differences near the surface (Figures 14i,
771 l), while positive and negative differences coexist over the lake, potentially reflecting
772 complex physicochemical mechanisms triggered by lake emissions. Figures S16g-l
773 show similar patterns at 23:00 and 05:00. In summary, these comparative experiments
774 confirm that treatment of lake emissions profoundly affects assessment of lake



775 environmental effects. Retaining lake emissions synergizes with physical accumulation
776 mechanisms to significantly amplify apparent daytime pollution enhancement, while
777 nighttime urban physical purification remains significant. Accurately characterizing
778 underlying surface emissions is crucial for correctly quantifying the dual role lakes play
779 through daytime pollution enhancement and nighttime purification.

780

781 **4. Conclusion and Discussion**

782 Lakes significantly alter local meteorological conditions through thermal
783 contrasts with surrounding surfaces, influencing air pollutant transport and
784 accumulation in adjacent urban areas. While extensive research has examined lake
785 effects on ozone, systematic investigation into lake impacts on PM_{2.5} and its
786 components remains lacking, particularly regarding coupling between lake-induced
787 physical processes (circulation, mixing, deposition) and chemical transformation. This
788 study systematically reveals lake effects on PM_{2.5} and its components within a lake-
789 urban system, elucidating regional PM_{2.5} evolution patterns through physical-chemical
790 coupling mechanisms under lake influence.

791 We investigated the lake effect on PM_{2.5} concentrations through high-resolution
792 WRF-Chem simulations with Lake and Nolake scenarios centered on the Lake Chaohu
793 and Hefei region. During daytime, the lake significantly enhances PM_{2.5} accumulation,
794 with concentrations over the lake surface exceeding those in the Nolake experiment by
795 more than 10-15 µg/m³ and reaching levels comparable to or higher than urban areas,
796 particularly at 14:00 LT when the pollution-enhancing effect peaks. This daytime
797 enhancement extends to surrounding urban areas, gradually weakening with distance.
798 Satellite observations validate this anomalous daytime accumulation over the lake
799 surface. During nighttime, however, the lake's impact fundamentally reverses, reducing
800 urban PM_{2.5} concentrations by approximately 10 µg/m³, with maximum purification
801 effects occurring 12-18 kilometers from the lakeshore rather than in immediately
802 adjacent areas. Notably, this diurnal reversal exhibits strong component-dependency.
803 Component analysis demonstrates that secondary PM_{2.5} dominates daytime pollution



804 enhancement, with increases of 5-10 $\mu\text{g}/\text{m}^3$ significantly exceeding primary $\text{PM}_{2.5}$
805 increases of 0-5 $\mu\text{g}/\text{m}^3$. The accumulation of secondary particles over the lake,
806 subsequently transported to urban areas by lake breeze, is a key mechanism worsening
807 urban daytime pollution. Conversely, nighttime purification is primarily driven by
808 physical removal of primary $\text{PM}_{2.5}$, with reductions exceeding 10 $\mu\text{g}/\text{m}^3$ in urban areas,
809 while secondary $\text{PM}_{2.5}$ reductions remain limited to 0-3 $\mu\text{g}/\text{m}^3$. These findings
810 demonstrate that lakes play a complex dual role in regulating regional air quality
811 through distinct physical-chemical mechanisms during day and night.

812 To elucidate the diurnal reversal mechanism, we analyzed the physical,
813 dynamical, and chemical drivers of $\text{PM}_{2.5}$ evolution. Lakes suppress boundary layer
814 development, reduce turbulent mixing, and decrease dry deposition velocity, with
815 effects persisting throughout the diurnal cycle but varying in intensity. These combined
816 effects extend $\text{PM}_{2.5}$ lifetimes by over 800 hours during daytime and approximately 500
817 hours during nighttime, effectively transforming lakes into particle “storage zones.”
818 Lake-land thermal contrasts drive distinct transport regimes during different periods.
819 During daytime, lake breeze-background wind interactions create convergence zones
820 along lakeshores that trap pollutants, increasing concentrations by up to 10 $\mu\text{g}/\text{m}^3$ from
821 the surface to nearly 1 km altitude. At night, land breeze circulation enhances urban
822 vertical mixing, purifying near-surface $\text{PM}_{2.5}$ by up to 16 $\mu\text{g}/\text{m}^3$ while elevating
823 concentrations aloft. This dual mechanism explains the diurnal reversal effect on urban
824 air quality. In addition, lakes regulate local temperature and humidity, suppressing
825 thermal decomposition of ammonium nitrate and other secondary aerosols, with
826 secondary $\text{PM}_{2.5}$ differences substantially exceeding those of primary particles. These
827 mechanisms operate synergistically to shape the complex spatiotemporal patterns of
828 lake-urban $\text{PM}_{2.5}$ interactions.

829 To assess the impact of emission inventory uncertainty on lake-urban $\text{PM}_{2.5}$
830 interactions, we conducted additional experiments (Lake_emis and Nolake_emis)
831 retaining the artificial emission settings over lake surfaces, as most inventories
832 erroneously assign anthropogenic emissions to lakes. Results show that emission
833 treatment profoundly affects lake effect assessments. During daytime, lake emissions



834 synergize with physical accumulation mechanisms to transform the lake area into a
835 prominent pollution hotspot with concentrations reaching 50-80 $\mu\text{g}/\text{m}^3$, exceeding
836 urban levels of 35-40 $\mu\text{g}/\text{m}^3$ at 14:00. Peak concentration differences approach 60 $\mu\text{g}/\text{m}^3$,
837 significantly amplifying the apparent pollution enhancement compared to the zero-
838 emission scenario. During nighttime, the lake-driven purification mechanism persists,
839 with near-surface urban concentration reductions reaching approximately 30 $\mu\text{g}/\text{m}^3$ at
840 20:00 and 20 $\mu\text{g}/\text{m}^3$ at 02:00. These findings confirm that accurate emission
841 characterization is crucial for quantifying lakes' complex role in regional air quality.
842 However, most current emission inventories lack sufficient spatial resolution to
843 distinguish water surfaces from land, often erroneously assigning anthropogenic
844 emissions to lake areas and biasing lake effect assessments. Developing emission
845 inventories that accurately characterize surface-specific emission patterns is crucial for
846 reliable assessment of lake-urban air quality interactions and effective pollution control
847 strategies.

848 While this study provides valuable insights into lake effects on $\text{PM}_{2.5}$
849 distributions, several considerations emerge regarding broader applicability and future
850 research directions. It is important to emphasize that while this study centers on the
851 Lake Chaohu and Hefei system, the identified mechanisms governing the diurnal
852 evolution of $\text{PM}_{2.5}$ are rooted in fundamental physical principles rather than site-
853 specific coincidences. The intrinsic properties of a lake surface, notably its high thermal
854 capacity and low aerodynamic roughness, are universal physical attributes that
855 consistently distinguish water bodies from terrestrial surfaces regardless of geographic
856 location. These characteristics drive the suppression of PBL development and
857 mechanical turbulence while leading to characteristically low dry deposition velocities.
858 Such processes collectively facilitate the formation of atmospheric storage zones that
859 prolong pollutant lifetimes and create potential pollution reservoirs over the water. At
860 night, the presence of the lake enhances turbulent mixing in the urban area, thereby
861 promoting the purification of near-surface pollutants in the adjacent city. Combined
862 with thermodynamic regulation of secondary aerosol formation, these surface contrasts
863 establish lakes as dual regulators that both enhance and purify pollution. This may



864 represents a widespread atmospheric phenomenon characteristic of urban-lake
865 interfaces globally rather than an isolated case. However, we acknowledge that the
866 specific manifestation and magnitude of these lake effects are modulated by local
867 environmental factors, such as topography, emission intensity, and background wind
868 fields. These conditions determine the precise horizontal and vertical redistribution of
869 pollutants and the exact location of convergence zones. Therefore, while our findings
870 provide a generalized framework for understanding lake-atmosphere-pollution
871 coupling, the exact impact in other regions remains dependent on the local
872 environmental configuration. By elucidating these universal physical drivers, this study
873 provides a transferable scientific basis for air quality assessment and forecasting in
874 lake-adjacent regions worldwide.

875 Furthermore, our investigation concentrated on PM_{2.5} and its components, yet
876 atmospheric pollution involves complex multi-species interactions. The transport
877 patterns of gaseous pollutants such as SO₂ and NO₂ within lake-land thermal circulation
878 systems, and their conversion to secondary particulate matter under lake modulation,
879 deserve comprehensive investigation. Extending analysis to other lake-urban systems
880 and conducting simultaneous multi-pollutant observations would enhance
881 understanding of lakes' integrated impacts on regional atmospheric chemistry,
882 providing scientific foundations for air quality management and multi-pollutant
883 synergistic control strategies in lake-adjacent regions globally. In addition, this study
884 focused on spring conditions, capturing typical lake thermal effects but not accounting
885 for seasonal variations that inevitably alter lake effect characteristics. Summer and
886 winter conditions may exhibit distinctly different thermal contrast patterns between
887 lake and land surfaces, directly influencing boundary layer structures, local circulation
888 intensities, and pollutant transport-dispersion patterns. Technical limitations also
889 present opportunities for improvement. Although this study employed high-resolution
890 1 km simulations, the fine-scale structures of lake-land boundary layers and mesoscale
891 phenomena such as lake-breeze fronts require even higher spatial resolution for
892 accurate representation. Current planetary boundary layer parameterization schemes
893 may contain uncertainties when handling complex surface conditions, particularly in



894 water-land transition zones. Future research should integrate more sophisticated
895 numerical methods, develop specialized parameterization schemes for lake-land
896 interface processes, and optimize dry deposition parameterizations across different
897 surface types based on expanded observational datasets to enhance model capabilities
898 in simulating lake micrometeorology and boundary layer dynamics.

899

900

901

902

903

904

905

906

907

908

909

910

911

912

913

914

915

916

917

918

919

920

921

922

923



924 **Code and data availability.** The updated USTC version of WRF-Chem can be
925 downloaded from <https://doi.org/10.5281/zenodo.15702248> or can be obtained from
926 the corresponding author upon request. The Multi-resolution Emission Inventory for
927 China (MEIC) at $0.25^\circ \times 0.25^\circ$ resolution for 2019 is available at
928 <http://meicmodel.org.cn> (last access: 11 August 2025) (Li et al., 2017a; Li et al., 2017b;
929 Zheng et al., 2018; Geng et al., 2024). The NCEP final reanalysis (FNL) data with a 1°
930 $\times 1^\circ$ resolution and 6 h temporal resolution are available at
931 <https://doi.org/10.5065/D6M043C6> (last access: 11 August 2025) (NCEP, 2000).

932

933 **Author contributions.** ZY, QY, and CZ designed the experiments and conducted
934 and analyzed the simulations. All authors contributed to the discussion and final version
935 of the paper.

936

937 **Competing interests.** The contact author has declared that none of the authors
938 has any competing interests.

939

940 **Disclaimer.** Publisher's note: Copernicus Publications remains neutral with
941 regard to jurisdictional claims made in the text, published maps, institutional affiliations,
942 or any other geographical representation in this paper. While Copernicus Publications
943 makes every effort to include appropriate place names, the final responsibility lies with
944 the authors.

945

946 **Acknowledgements.** This research was supported by the National Key Scientific
947 and Technological Infrastructure project "Earth System Numerical Simulation Facility"
948 (EarthLab). The study used computing resources from the Supercomputing Center of
949 the University of Science and Technology of China (USTC) and the Qingdao
950 Supercomputing and Big Data Center.

951

952 **Financial support.** This research has been supported by the National Key
953 Research and Development Program of China (grant no. 2022YFC3700701), the



954 Strategic Priority Research Program of the Chinese Academy of Sciences (grant no.
955 XDB0500303), the National Natural Science Foundation of China (grant no. 41775146),
956 the USTC Research Funds of the Double First-Class Initiative (grant nos.
957 YD2080002007 and KY2080000114), the Science and Technology Innovation Project
958 of Laoshan Laboratory (grant no. LSKJ202300305), the National Natural Science
959 Foundation of China (NSFC) Young Students' Basic Research Project (Doctoral
960 Candidates, grant no. 424B2042), the Innovation Group Project of Southern Marine
961 Science and Engineering Guangdong Laboratory (Zhuhai) (grant no. 311024009), and
962 the Southern Marine Science and Engineering Guangdong Laboratory (Zhuhai) (grant
963 no. SML2024SP011).

964

965

966

967

968

969

970

971

972

973

974

975

976

977

978

979

980

981

982



983 **Reference**

- 984 Atkinson, B. W.: Meso-scale atmospheric circulations, Academic Press, London, 495
985 pp.,1981.
- 986 Binkowski, F. S. and Shankar, U.: The Regional Particulate Matter Model .1. Model
987 description and preliminary results, Journal of Geophysical Research-
988 Atmospheres, 100, 26191-26209, <https://doi.org/10.1029/95jd02093>, 1995.
- 989 Brook, J. R., Makar, P. A., Sills, D. M. L., Hayden, K. L., and McLaren, R.: Exploring
990 the nature of air quality over southwestern Ontario: main findings from the Border
991 Air Quality and Meteorology Study, Atmospheric Chemistry and Physics, 13,
992 10461-10482, <https://doi.org/10.5194/acp-13-10461-2013>, 2013.
- 993 Burley, J. D., Theiss, S., Bytnerowicz, A., Gertler, A., Schilling, S., and Zielinska, B.:
994 Surface ozone in the Lake Tahoe Basin, Atmospheric Environment, 109, 351-369,
995 <https://doi.org/10.1016/j.atmosenv.2015.02.001>, 2015.
- 996 Capps, S. L., Hu, Y., and Russell, A. G.: Assessing Near-Field and Downwind Impacts
997 of Reactivity-Based Substitutions, Journal of the Air & Waste Management
998 Association, 60, 316-327, <https://doi.org/10.3155/1047-3289.60.3.316>, 2010.
- 999 Chai, F., Gao, J., Chen, Z., Wang, S., Zhang, Y., Zhang, J., Zhang, H., Yun, Y., and Ren,
1000 C.: Spatial and temporal variation of particulate matter and gaseous pollutants in
1001 26 cities in China, Journal of Environmental Sciences, 26, 75-82,
1002 [https://doi.org/10.1016/s1001-0742\(13\)60383-6](https://doi.org/10.1016/s1001-0742(13)60383-6), 2014.
- 1003 Chapman, E. G., Gustafson, W. I., Jr., Easter, R. C., Barnard, J. C., Ghan, S. J., Pekour,
1004 M. S., and Fast, J. D.: Coupling aerosol-cloud-radiative processes in the WRF-
1005 Chem model: Investigating the radiative impact of elevated point sources,
1006 Atmospheric Chemistry and Physics, 9, 945-964, [https://doi.org/10.5194/acp-9-
1007 945-2009](https://doi.org/10.5194/acp-9-945-2009), 2009.
- 1008 Chen, F. and Dudhia, J.: Coupling an Advanced Land Surface–Hydrology Model with
1009 the Penn State–NCAR MM5 Modeling System. Part I: Model Implementation and
1010 Sensitivity, Monthly Weather Review, 129, 569-585, 2001.
- 1011 Chen, J. and Hoek, G.: Long-term exposure to PM and all-cause and cause-specific



- 1012 mortality: A systematic review and meta-analysis, *Environment International*, 143,
1013 <https://doi.org/10.1016/j.envint.2020.105974>, 2020.
- 1014 Chen, X., Chen, Y., Shimizu, T., Niu, J., Nakagami, K. i., Qian, X., Jia, B., Nakajima,
1015 J., Han, J., and Li, J.: Water resources management in the urban agglomeration of
1016 the Lake Biwa region, Japan: An ecosystem services-based sustainability
1017 assessment, *Science of the Total Environment*, 586, 174-187,
1018 <https://doi.org/10.1016/j.scitotenv.2017.01.197>, 2017.
- 1019 Dentener, F., Kinne, S., Bond, T., Boucher, O., Cofala, J., Generoso, S., Ginoux, P.,
1020 Gong, S., Hoelzemann, J. J., Ito, A., Marelli, L., Penner, J. E., Putaud, J. P., Textor,
1021 C., Schulz, M., van der Werf, G. R., and Wilson, J.: Emissions of primary aerosol
1022 and precursor gases in the years 2000 and 1750 prescribed data-sets for AeroCom,
1023 *Atmospheric Chemistry and Physics*, 6, 4321-4344, [https://doi.org/10.5194/acp-6-](https://doi.org/10.5194/acp-6-4321-2006)
1024 [4321-2006](https://doi.org/10.5194/acp-6-4321-2006), 2006.
- 1025 Du, Q., Zhao, C., Zhang, M., Dong, X., Chen, Y., Liu, Z., Hu, Z., Zhang, Q., Li, Y.,
1026 Yuan, R., and Miao, S.: Modeling diurnal variation of surface PM_{2.5} concentrations
1027 over East China with WRF-Chem: impacts from boundary-layer mixing and
1028 anthropogenic emission, *Atmospheric Chemistry and Physics*, 20, 2839-2863,
1029 <https://doi.org/10.5194/acp-20-2839-2020>, 2020.
- 1030 Dye, T. S., Roberts, P. T., and Korc, M. E.: OBSERVATIONS OF TRANSPORT
1031 PROCESSES FOR OZONE AND OZONE PRECURSORS DURING THE 1991
1032 LAKE-MICHIGAN OZONE STUDY, *Journal of Applied Meteorology*, 34, 1877-
1033 1889, [https://doi.org/10.1175/1520-0450\(1995\)034<1877:Ootpfo>2.0.Co;2](https://doi.org/10.1175/1520-0450(1995)034<1877:Ootpfo>2.0.Co;2), 1995.
- 1034 Fast, J. D. and Heilman, W. E.: Simulated sensitivity of seasonal ozone exposure in the
1035 Great Lakes region to changes in anthropogenic emissions in the presence of
1036 interannual variability, *Atmospheric Environment*, 39, 5291-5306,
1037 <https://doi.org/10.1016/j.atmosenv.2005.05.032>, 2005.
- 1038 Fosco, T. and Schmeling, M.: Aerosol ion concentration dependence on atmospheric
1039 conditions in Chicago, *Atmospheric Environment*, 40, 6638-6649,
1040 <https://doi.org/10.1016/j.atmosenv.2006.05.061>, 2006.
- 1041 Garratt, J. R.: THE INTERNAL BOUNDARY-LAYER - A REVIEW, *Boundary-Layer*



- 1042 Meteorology, 50, 171-203, <https://doi.org/10.1007/bf00120524>, 1990.
- 1043 Geng, G., Liu, Y., Liu, Y., Liu, S., Cheng, J., Yan, L., Wu, N., Hu, H., Tong, D., Zheng,
1044 B., Yin, Z., He, K., and Zhang, Q.: Efficacy of China's clean air actions to tackle
1045 PM_{2.5} pollution between 2013 and 2020, Nature Geoscience, 17,
1046 <https://doi.org/10.1038/s41561-024-01540-z>, 2024.
- 1047 Guo, H., Cheng, T., Gu, X., Wang, Y., Chen, H., Bao, F., Shi, S., Xu, B., Wang, W., Zuo,
1048 X., Zhang, X., and Meng, C.: Assessment of PM_{2.5} concentrations and exposure
1049 throughout China using ground observations, Science of the Total Environment,
1050 601, 1024-1030, <https://doi.org/10.1016/j.scitotenv.2017.05.263>, 2017.
- 1051 Guo, J., Deng, M., Lee, S. S., Wang, F., Li, Z., Zhai, P., Liu, H., Lv, W., Yao, W., and
1052 Li, X.: Delaying precipitation and lightning by air pollution over the Pearl River
1053 Delta. Part I: Observational analyses, Journal of Geophysical Research-
1054 Atmospheres, 121, 6472-6488, <https://doi.org/10.1002/2015jd023257>, 2016.
- 1055 Guo, S., Hu, M., Zamora, M. L., Peng, J., Shang, D., Zheng, J., Du, Z., Wu, Z., Shao,
1056 M., Zeng, L., Molina, M. J., and Zhang, R.: Elucidating severe urban haze
1057 formation in China, Proceedings of the National Academy of Sciences of the
1058 United States of America, 111, 17373-17378,
1059 <https://doi.org/10.1073/pnas.1419604111>, 2014.
- 1060 Gustafson, W. I., Jr., Chapman, E. G., Ghan, S. J., Easter, R. C., and Fast, J. D.: Impact
1061 on modeled cloud characteristics due to simplified treatment of uniform cloud
1062 condensation nuclei during NEAQS 2004, Geophysical Research Letters, 34,
1063 <https://doi.org/10.1029/2007gl030021>, 2007.
- 1064 Harris, L. and Kotamarthi, V. R.: The characteristics of the Chicago Lake breeze and
1065 its effects on trace particle transport: Results from an episodic event simulation,
1066 Journal of Applied Meteorology, 44, 1637-1654,
1067 <https://doi.org/10.1175/jam2301.1>, 2005.
- 1068 Hayden, K. L., Sills, D. M. L., Brook, J. R., Li, S. M., Makar, P. A., Markovic, M. Z.,
1069 Liu, P., Anlauf, K. G., O'Brien, J. M., Li, Q., and McLaren, R.: Aircraft study of
1070 the impact of lake-breeze circulations on trace gases and particles during BAQS-
1071 Met 2007, Atmospheric Chemistry and Physics, 11, 10173-10192,



- 1072 <https://doi.org/10.5194/acp-11-10173-2011>, 2011.
- 1073 He, J., Gong, S., Yu, Y., Yu, L., Wu, L., Mao, H., Song, C., Zhao, S., Liu, H., Li, X.,
1074 and Li, R.: Air pollution characteristics and their relation to meteorological
1075 conditions during 2014-2015 in major Chinese cities, *Environmental Pollution*,
1076 223, 484-496, <https://doi.org/10.1016/j.envpol.2017.01.050>, 2017.
- 1077 Ho, H. C., Wong, M. S., Yang, L., Shi, W., Yang, J., Bilal, M., and Chan, T.-C.:
1078 Spatiotemporal influence of temperature, air quality, and urban environment on
1079 cause-specific mortality during hazy days, *Environment International*, 112, 10-22,
1080 <https://doi.org/10.1016/j.envint.2017.12.001>, 2018.
- 1081 Hong, S.-Y., Noh, Y., and Dudhia, J.: A new vertical diffusion package with an explicit
1082 treatment of entrainment processes, *Monthly Weather Review*, 134, 2318-2341,
1083 <https://doi.org/10.1175/mwr3199.1>, 2006.
- 1084 Hu, J., Wang, Y., Ying, Q., and Zhang, H.: Spatial and temporal variability of
1085 $PM_{2.5}$ and PM_{10} over the North China Plain and the
1086 Yangtze River Delta, China, *Atmospheric Environment*, 95, 598-609,
1087 <https://doi.org/10.1016/j.atmosenv.2014.07.019>, 2014a.
- 1088 Hu, J., Zhang, H., Chen, S., Ying, Q., Wiedinmyer, C., Vandenberghe, F., and Kleeman,
1089 M. J.: Identifying $PM_{2.5}$ and $PM_{0.1}$ Sources for Epidemiological Studies in
1090 California, *Environmental Science & Technology*, 48, 4980-4990,
1091 <https://doi.org/10.1021/es404810z>, 2014b.
- 1092 Hu, L. and Li, Q.: Greenspace, bluespace, and their interactive influence on urban
1093 thermal environments, *Environmental Research Letters*, 15,
1094 <https://doi.org/10.1088/1748-9326/ab6c30>, 2020.
- 1095 Hu, X.-M. and Xue, M.: Influence of Synoptic Sea-Breeze Fronts on the Urban Heat
1096 Island Intensity in Dallas-Fort Worth, Texas, *Monthly Weather Review*, 144, 1487-
1097 1507, <https://doi.org/10.1175/mwr-d-15-0201.1>, 2016.
- 1098 Hu, X.-M., Ma, Z., Lin, W., Zhang, H., Hu, J., Wang, Y., Xu, X., Fuentes, J. D., and
1099 Xue, M.: Impact of the Loess Plateau on the atmospheric boundary layer structure
1100 and air quality in the North China Plain: A case study, *Science of the Total
1101 Environment*, 499, 228-237, <https://doi.org/10.1016/j.scitotenv.2014.08.053>,



- 1102 2014c.
- 1103 Hu, Z., Huang, J., Zhao, C., Bi, J., Jin, Q., Qian, Y., Leung, L. R., Feng, T., Chen, S.,
1104 and Ma, J.: Modeling the contributions of Northern Hemisphere dust sources to
1105 dust outflow from East Asia, *Atmospheric Environment*, 202, 234-243,
1106 <https://doi.org/10.1016/j.atmosenv.2019.01.022>, 2019.
- 1107 Huang, R.-J., Zhang, Y., Bozzetti, C., Ho, K.-F., Cao, J.-J., Han, Y., Daellenbach, K. R.,
1108 Slowik, J. G., Platt, S. M., Canonaco, F., Zotter, P., Wolf, R., Pieber, S. M., Bruns,
1109 E. A., Crippa, M., Ciarelli, G., Piazzalunga, A., Schwikowski, M., Abbaszade, G.,
1110 Schnelle-Kreis, J., Zimmermann, R., An, Z., Szidat, S., Baltensperger, U., El
1111 Haddad, I., and Prevot, A. S. H.: High secondary aerosol contribution to particulate
1112 pollution during haze events in China, *Nature*, 514, 218-222,
1113 <https://doi.org/10.1038/nature13774>, 2014.
- 1114 Iacono, M. J., Mlawer, E. J., Clough, S. A., and Morcrette, J. J.: Impact of an improved
1115 longwave radiation model, RRTM, on the energy budget and thermodynamic
1116 properties of the NCAR community climate model, CCM3, *Journal of Geophysical
1117 Research-Atmospheres*, 105, 14873-14890, <https://doi.org/10.1029/2000jd900091>,
1118 2000.
- 1119 Janssens-Maenhout, G., Crippa, M., Guizzardi, D., Dentener, F., Muntean, M., Pouliot,
1120 G., Keating, T., Zhang, Q., Kurokawa, J., Wankmueller, R., van der Gon, H. D.,
1121 Kuenen, J. J. P., Klimont, Z., Frost, G., Darras, S., Koffi, B., and Li, M.:
1122 HTAP_v2.2: a mosaic of regional and global emission grid maps for 2008 and 2010
1123 to study hemispheric transport of air pollution, *Atmospheric Chemistry and
1124 Physics*, 15, 11411-11432, <https://doi.org/10.5194/acp-15-11411-2015>, 2015.
- 1125 Jiang, Z., Huo, F., Ma, H., Song, J., and Dai, A.: Impact of Chinese Urbanization and
1126 Aerosol Emissions on the East Asian Summer Monsoon, *Journal of Climate*, 30,
1127 1019-1039, <https://doi.org/10.1175/jcli-d-15-0593.1>, 2017.
- 1128 Kain, J. S.: The Kain-Fritsch convective parameterization: An update, *Journal of
1129 Applied Meteorology*, 43, 170-181, [https://doi.org/10.1175/1520-
1130 0450\(2004\)043<0170:Tkcpau>2.0.Co;2](https://doi.org/10.1175/1520-0450(2004)043<0170:Tkcpau>2.0.Co;2), 2004.
- 1131 Lei, Y., Zhang, Q., He, K. B., and Streets, D. G.: Primary anthropogenic aerosol



- 1132 emission trends for China, 1990-2005, *Atmospheric Chemistry and Physics*, 11,
1133 931-954, <https://doi.org/10.5194/acp-11-931-2011>, 2011.
- 1134 Levy, I., Dayan, U., and Mahrer, Y.: A five-year study of coastal recirculation and its
1135 effect on air pollutants over the East Mediterranean region, *Journal of Geophysical*
1136 *Research-Atmospheres*, 113, <https://doi.org/10.1029/2007jd009529>, 2008.
- 1137 Levy, I., Makar, P. A., Sills, D., Zhang, J., Hayden, K. L., Mihele, C., Narayan, J.,
1138 Moran, M. D., Sjostedt, S., and Brook, J.: Unraveling the complex local-scale
1139 flows influencing ozone patterns in the southern Great Lakes of North America,
1140 *Atmospheric Chemistry and Physics*, 10, 10895-10915,
1141 <https://doi.org/10.5194/acp-10-10895-2010>, 2010.
- 1142 Li, H., Ren, G., and Li, W.: Diurnal and intra-season variation of warm-season
1143 temperature in coastal zone of Qinghai Lake, *Theoretical and Applied Climatology*,
1144 138, 1203-1217, <https://doi.org/10.1007/s00704-019-02893-x>, 2019.
- 1145 Li, M., Liu, H., Geng, G., Hong, C., Liu, F., Song, Y., Tong, D., Zheng, B., Cui, H.,
1146 Man, H., Zhang, Q., and He, K.: Anthropogenic emission inventories in China: a
1147 review, *National Science Review*, 4, 834-866, <https://doi.org/10.1093/nsr/nwx150>,
1148 2017a.
- 1149 Li, M., Zhang, Q., Kurokawa, J.-i., Woo, J.-H., He, K., Lu, Z., Ohara, T., Song, Y.,
1150 Streets, D. G., Carmichael, G. R., Cheng, Y., Hong, C., Huo, H., Jiang, X., Kang,
1151 S., Liu, F., Su, H., and Zheng, B.: MIX: a mosaic Asian anthropogenic emission
1152 inventory under the international collaboration framework of the MICS-Asia and
1153 HTAP, *Atmospheric Chemistry and Physics*, 17, 935-963,
1154 <https://doi.org/10.5194/acp-17-935-2017>, 2017b.
- 1155 Li, Y., An, J., and Gultepe, I.: Effects of Additional HONO Sources on Visibility over
1156 the North China Plain, *Advances in Atmospheric Sciences*, 31, 1221-1232,
1157 <https://doi.org/10.1007/s00376-014-4019-1>, 2014.
- 1158 Li, Z., Guo, J., Ding, A., Liao, H., Liu, J., Sun, Y., Wang, T., Xue, H., Zhang, H., and
1159 Zhu, B.: Aerosol and boundary-layer interactions and impact on air quality,
1160 *National Science Review*, 4, 810-833, <https://doi.org/10.1093/nsr/nwx117>, 2017c.
- 1161 Li, Z., Li, C., Chen, H., Tsay, S. C., Holben, B., Huang, J., Li, B., Maring, H., Qian, Y.,



- 1162 Shi, G., Xia, X., Yin, Y., Zheng, Y., and Zhuang, G.: East Asian Studies of
1163 Tropospheric Aerosols and their Impact on Regional Climate (EAST-AIRC): An
1164 overview, *Journal of Geophysical Research-Atmospheres*, 116,
1165 <https://doi.org/10.1029/2010jd015257>, 2011.
- 1166 Li, Z., Lau, W. K. M., Ramanathan, V., Wu, G., Ding, Y., Manoj, M. G., Liu, J., Qian,
1167 Y., Li, J., Zhou, T., Fan, J., Rosenfeld, D., Ming, Y., Wang, Y., Huang, J., Wang, B.,
1168 Xu, X., Lee, S. S., Cribb, M., Zhang, F., Yang, X., Zhao, C., Takemura, T., Wang,
1169 K., Xia, X., Yin, Y., Zhang, H., Guo, J., Zhai, P. M., Sugimoto, N., Babu, S. S., and
1170 Brasseur, G. P.: Aerosol and monsoon climate interactions over Asia, *Reviews of*
1171 *Geophysics*, 54, 866-929, <https://doi.org/10.1002/2015rg000500>, 2016.
- 1172 Liu, S., Liu, Z., Li, J., Wang, Y., Ma, Y., Sheng, L., Liu, H., Liang, F., Xin, G., and
1173 Wang, J.: Numerical simulation for the coupling effect of local atmospheric
1174 circulations over the area of Beijing, Tianjin and Hebei Province, *Science in China*
1175 *Series D-Earth Sciences*, 52, 382-392, <https://doi.org/10.1007/s11430-009-0030-2>,
1176 2009.
- 1177 Liu, X. G., Li, J., Qu, Y., Han, T., Hou, L., Gu, J., Chen, C., Yang, Y., Liu, X., Yang, T.,
1178 Zhang, Y., Tian, H., and Hu, M.: Formation and evolution mechanism of regional
1179 haze: a case study in the megacity Beijing, China, *Atmospheric Chemistry and*
1180 *Physics*, 13, 4501-4514, <https://doi.org/10.5194/acp-13-4501-2013>, 2013.
- 1181 Liu, Z., Gao, W., Yu, Y., Hu, B., Xin, J., Sun, Y., Wang, L., Wang, G., Bi, X., Zhang,
1182 G., Xu, H., Cong, Z., He, J., Xu, J., and Wang, Y.: Characteristics of PM_{2.5} mass
1183 concentrations and chemical species in urban and background areas of China:
1184 emerging results from the CARE-China network, *Atmospheric Chemistry and*
1185 *Physics*, 18, 8849-8871, <https://doi.org/10.5194/acp-18-8849-2018>, 2018.
- 1186 Lu, D., Xu, J., Yang, D., and Zhao, J.: Spatio-temporal variation and influence factors
1187 of PM_{2.5} concentrations in China from 1998 to 2014, *Atmospheric Pollution*
1188 *Research*, 8, 1151-1159, <https://doi.org/10.1016/j.apr.2017.05.005>, 2017.
- 1189 Lyons, W. A.: The climatology and prediction of the Chicago lake breeze, *Journal of*
1190 *Applied Meteorology and Climatology*, 11, 1259-1270, 1972.
- 1191 Lyons, W. A. and Olsson, L. E.: Detailed mesometeorological studies of air pollution



- 1192 dispersion in the Chicago lake breeze, Monthly Weather Review, 101, 387-403,
1193 1973.
- 1194 Lyons, W. A., Pielke, R. A., Tremback, C. J., Walko, R. L., Moon, D. A., and Keen, C.
1195 S.: MODELING IMPACTS OF MESOSCALE VERTICAL MOTIONS UPON
1196 COASTAL ZONE AIR-POLLUTION DISPERSION, Atmospheric Environment,
1197 29, 283-301, [https://doi.org/10.1016/1352-2310\(94\)00217-9](https://doi.org/10.1016/1352-2310(94)00217-9), 1995.
- 1198 Ma, Y., Chen, R., Pan, G., Xu, X., Song, W., Chen, B., and Kan, H.: Fine particulate air
1199 pollution and daily mortality in Shenyang, China, Science of the Total
1200 Environment, 409, 2473-2477, <https://doi.org/10.1016/j.scitotenv.2011.03.017>,
1201 2011.
- 1202 Makar, P. A., Zhang, J., Gong, W., Stroud, C., Sills, D., Hayden, K. L., Brook, J., Levy,
1203 I., Mihele, C., Moran, M. D., Tarasick, D. W., He, H., and Plummer, D.: Mass
1204 tracking for chemical analysis: the causes of ozone formation in southern Ontario
1205 during BAQS-Met 2007, Atmospheric Chemistry and Physics, 10, 11151-11173,
1206 <https://doi.org/10.5194/acp-10-11151-2010>, 2010.
- 1207 Miao, Y., Liu, S., Zheng, Y., and Wang, S.: Modeling the feedback between aerosol and
1208 boundary layer processes: a case study in Beijing, China, Environmental Science
1209 and Pollution Research, 23, 3342-3357, [https://doi.org/10.1007/s11356-015-5562-](https://doi.org/10.1007/s11356-015-5562-8)
1210 [8](https://doi.org/10.1007/s11356-015-5562-8), 2016.
- 1211 Miao, Y., Liu, S., Chen, B., Zhang, B., Wang, S., and Li, S.: Simulating urban flow and
1212 dispersion in Beijing by coupling a CFD model with the WRF model, Advances in
1213 Atmospheric Sciences, 30, 1663-1678, [https://doi.org/10.1007/s00376-013-2234-](https://doi.org/10.1007/s00376-013-2234-9)
1214 [9](https://doi.org/10.1007/s00376-013-2234-9), 2013.
- 1215 Miao, Y., Liu, S., Zheng, Y., Wang, S., Liu, Z., and Zhang, B.: Numerical study of the
1216 effects of Planetary Boundary Layer structure on the pollutant dispersion within
1217 built-up areas, Journal of Environmental Sciences, 32, 168-179,
1218 <https://doi.org/10.1016/j.jes.2014.10.025>, 2015.
- 1219 Miao, Y., Guo, J., Liu, S., Liu, H., Li, Z., Zhang, W., and Zhai, P.: Classification of
1220 summertime synoptic patterns in Beijing and their associations with boundary
1221 layer structure affecting aerosol pollution, Atmospheric Chemistry and Physics, 17,



- 1222 3097-3110, <https://doi.org/10.5194/acp-17-3097-2017>, 2017.
- 1223 Mlawer, E. J., Taubman, S. J., Brown, P. D., Iacono, M. J., and Clough, S. A.: Radiative
1224 transfer for inhomogeneous atmospheres: RRTM, a validated correlated-k model
1225 for the longwave, *Journal of Geophysical Research-Atmospheres*, 102, 16663-
1226 16682, <https://doi.org/10.1029/97jd00237>, 1997.
- 1227 Monks, P. S., Archibald, A. T., Colette, A., Cooper, O., Coyle, M., Derwent, R., Fowler,
1228 D., Granier, C., Law, K. S., Mills, G. E., Stevenson, D. S., Tarasova, O., Thouret,
1229 V., von Schneidemesser, E., Sommariva, R., Wild, O., and Williams, M. L.:
1230 Tropospheric ozone and its precursors from the urban to the global scale from air
1231 quality to short-lived climate forcer, *Atmospheric Chemistry and Physics*, 15,
1232 8889-8973, <https://doi.org/10.5194/acp-15-8889-2015>, 2015.
- 1233 Morrison, H., Thompson, G., and Tatarskii, V.: Impact of Cloud Microphysics on the
1234 Development of Trailing Stratiform Precipitation in a Simulated Squall Line:
1235 Comparison of One- and Two-Moment Schemes, *Monthly Weather Review*, 137,
1236 991-1007, <https://doi.org/10.1175/2008mwr2556.1>, 2009.
- 1237 NCEP: NCEP FNL operational model global tropospheric analyses, continuing from
1238 July 1999, Research Data Archive at the National Center for Atmospheric
1239 Research, Computational and Information Systems Laboratory [data set],
1240 <https://doi.org/https://doi.org/10.5065/D6M043C6>, 2000.
- 1241 Peng, J., Huang, Y., Liu, T., Jiang, L., Xu, Z., Xing, W., Feng, X., and De Maeyer, P.:
1242 Atmospheric nitrogen pollution in urban agglomeration and its impact on alpine
1243 lake-case study of Tianchi Lake, *Science of the Total Environment*, 688, 312-323,
1244 <https://doi.org/10.1016/j.scitotenv.2019.06.202>, 2019.
- 1245 Sills, D. M. L., Brook, J. R., Levy, I., Makar, P. A., Zhang, J., and Taylor, P. A.: Lake
1246 breezes in the southern Great Lakes region and their influence during BAQS-Met
1247 2007, *Atmospheric Chemistry and Physics*, 11, 7955-7973,
1248 <https://doi.org/10.5194/acp-11-7955-2011>, 2011.
- 1249 Steiner, A. L., Mermelstein, D., Cheng, S. J., Twine, T. E., and Oliphant, A.: Observed
1250 Impact of Atmospheric Aerosols on the Surface Energy Budget, *Earth Interactions*,
1251 17, <https://doi.org/10.1175/2013ei000523.1>, 2013.



- 1252 Stull, R. B.: An Introduction to Boundary Layer Meteorology, Springer Nether
1253 lands, 1988.
- 1254 Unger, N., Menon, S., Koch, D. M., and Shindell, D. T.: Impacts of aerosol-cloud
1255 interactions on past and future changes in tropospheric composition, Atmospheric
1256 Chemistry and Physics, 9, 4115-4129, <https://doi.org/10.5194/acp-9-4115-2009>,
1257 2009.
- 1258 Wang, F., Wang, Y., and Gao, M.: Impact of lake-atmosphere exchange on summertime
1259 ozone in the Lake Taihu region, Atmospheric Environment, 300,
1260 <https://doi.org/10.1016/j.atmosenv.2023.119664>, 2023.
- 1261 Wang, Y., Ying, Q., Hu, J., and Zhang, H.: Spatial and temporal variations of six criteria
1262 air pollutants in 31 provincial capital cities in China during 2013-2014,
1263 Environment International, 73, 413-422,
1264 <https://doi.org/10.1016/j.envint.2014.08.016>, 2014.
- 1265 Wang, Y., Gao, Y., Qin, H., Huang, J., Liu, C., Hu, C., Wang, W., Liu, S., and Lee, X.:
1266 Spatiotemporal Characteristics of Lake Breezes over Lake Taihu, China, Journal
1267 of Applied Meteorology and Climatology, 56, 2053-2065,
1268 <https://doi.org/10.1175/jamc-d-16-0220.1>, 2017.
- 1269 Wei, J., Li, Z., Pinker, R. T., Wang, J., Sun, L., Xue, W., Li, R., and Cribb, M.:
1270 Himawari-8-derived diurnal variations in ground-level PM_{2.5} pollution across
1271 China using the fast space-time Light Gradient Boosting Machine (LightGBM),
1272 Atmospheric Chemistry and Physics, 21, 7863-7880, [https://doi.org/10.5194/acp-
1273 21-7863-2021](https://doi.org/10.5194/acp-21-7863-2021), 2021.
- 1274 Wentworth, G. R., Murphy, J. G., and Sills, D. M. L.: Impact of lake breezes on ozone
1275 and nitrogen oxides in the Greater Toronto Area, Atmospheric Environment, 109,
1276 52-60, <https://doi.org/10.1016/j.atmosenv.2015.03.002>, 2015.
- 1277 Wiedinmyer, C., Akagi, S. K., Yokelson, R. J., Emmons, L. K., Al-Saadi, J. A., Orlando,
1278 J. J., and Soja, A. J.: The Fire INventory from NCAR (FINN): a high resolution
1279 global model to estimate the emissions from open burning, Geoscientific Model
1280 Development, 4, 625-641, <https://doi.org/10.5194/gmd-4-625-2011>, 2011.
- 1281 Wild, O., Zhu, X., and Prather, M. J.: Fast-j: Accurate simulation of in- and below-



- 1282 cloud photolysis in tropospheric chemical models, *Journal of Atmospheric*
1283 *Chemistry*, 37, 245-282, <https://doi.org/10.1023/a:1006415919030>, 2000.
- 1284 WRAP – Western Regional Air Partnership: 2002 Fire Emission Inventory for the
1285 WRAP Region – Phase II, Project No.178-6, available at:
1286 <http://www.wrapair.org/forums/fej/tasks/FEJFtask7PhaseII.html> (last access: 30
1287 September 2021), 2005.
- 1288 Yang, Y., Ruan, Z., Wang, X., Yang, Y., Mason, T. G., Lin, H., and Tian, L.: Short-term
1289 and long-term exposures to fine particulate matter constituents and health: A
1290 systematic review and meta-analysis, *Environmental Pollution*, 247, 874-882,
1291 <https://doi.org/10.1016/j.envpol.2018.12.060>, 2019.
- 1292 Yang, Z. N., Du, Q. Y., Yang, Q. K., Zhao, C., Li, G. D. Z., Xia, Z. H., Xu, M. Y., Yuan,
1293 R. M., Li, Y. B., Xia, K. H., Gu, J., and Feng, J. W.: Modeling urban pollutant
1294 transport at multiple resolutions: impacts of turbulent mixing, *Atmospheric*
1295 *Chemistry and Physics*, 25, 8831-8857, <https://doi.org/10.5194/acp-25-8831-2025>,
1296 2025.
- 1297 Ye, X., Song, Y., Cai, X., and Zhang, H.: Study on the synoptic flow patterns and
1298 boundary layer process of the severe haze events over the North China Plain in
1299 January 2013, *Atmospheric Environment*, 124, 129-145,
1300 <https://doi.org/10.1016/j.atmosenv.2015.06.011>, 2016.
- 1301 Yue, X., Ma, N. L., Sonne, C., Guan, R., Lam, S. S., Le, Q. V., Chen, X., Yang, Y., Gu,
1302 H., Rinklebe, J., and Peng, W.: Mitigation of indoor air pollution: A review of
1303 recent advances in adsorption materials and catalytic oxidation, *Journal of*
1304 *Hazardous Materials*, 405, <https://doi.org/10.1016/j.jhazmat.2020.124138>, 2021.
- 1305 Zaveri, R. A. and Peters, L. K.: A new lumped structure photochemical mechanism for
1306 large-scale applications, *Journal of Geophysical Research-Atmospheres*, 104,
1307 30387-30415, <https://doi.org/10.1029/1999jd900876>, 1999.
- 1308 Zhang, H., Wang, Y., Hu, J., Ying, Q., and Hu, X.-M.: Relationships between
1309 meteorological parameters and criteria air pollutants in three megacities in China,
1310 *Environmental Research*, 140, 242-254,
1311 <https://doi.org/10.1016/j.envres.2015.04.004>, 2015a.



- 1312 Zhang, L., Zhu, B., Gao, J., and Kang, H.: Impact of Taihu Lake on city ozone in the
1313 Yangtze River Delta, *Advances in Atmospheric Sciences*, 34, 226-234,
1314 <https://doi.org/10.1007/s00376-016-6099-6>, 2017.
- 1315 Zhang, M., Zhao, C., Yang, Y., Du, Q., Shen, Y., Lin, S., Gu, D., Su, W., and Liu, C.:
1316 Modeling sensitivities of BVOCs to different versions of MEGAN emission
1317 schemes in WRF-Chem (v3.6) and its impacts over eastern China, *Geoscientific
1318 Model Development*, 14, 6155-6175, <https://doi.org/10.5194/gmd-14-6155-2021>,
1319 2021.
- 1320 Zhang, R., Wang, G., Guo, S., Zarnora, M. L., Ying, Q., Lin, Y., Wang, W., Hu, M., and
1321 Wang, Y.: Formation of Urban Fine Particulate Matter, *Chemical Reviews*, 115,
1322 3803-3855, <https://doi.org/10.1021/acs.chemrev.5b00067>, 2015b.
- 1323 Zhang, R., Jing, J., Tao, J., Hsu, S. C., Wang, G., Cao, J., Lee, C. S. L., Zhu, L., Chen,
1324 Z., Zhao, Y., and Shen, Z.: Chemical characterization and source apportionment of
1325 PM_{2.5} in Beijing: seasonal perspective, *Atmospheric Chemistry and Physics*, 13,
1326 7053-7074, <https://doi.org/10.5194/acp-13-7053-2013>, 2013.
- 1327 Zhang, X. Y., Wang, Y. Q., Niu, T., Zhang, X. C., Gong, S. L., Zhang, Y. M., and Sun,
1328 J. Y.: Atmospheric aerosol compositions in China: spatial/temporal variability,
1329 chemical signature, regional haze distribution and comparisons with global
1330 aerosols, *Atmospheric Chemistry and Physics*, 12, 779-799,
1331 <https://doi.org/10.5194/acp-12-779-2012>, 2012.
- 1332 Zhao, C., Liu, X., Leung, L. R., and Hagos, S.: Radiative impact of mineral dust on
1333 monsoon precipitation variability over West Africa, *Atmospheric Chemistry and
1334 Physics*, 11, 1879-1893, <https://doi.org/10.5194/acp-11-1879-2011>, 2011.
- 1335 Zhao, C., Leung, L. R., Easter, R., Hand, J., and Avise, J.: Characterization of speciated
1336 aerosol direct radiative forcing over California, *Journal of Geophysical Research-
1337 Atmospheres*, 118, 2372-2388, <https://doi.org/10.1029/2012jd018364>, 2013a.
- 1338 Zhao, C., Chen, S., Leung, L. R., Qian, Y., Kok, J. F., Zaveri, R. A., and Huang, J.:
1339 Uncertainty in modeling dust mass balance and radiative forcing from size
1340 parameterization, *Atmospheric Chemistry and Physics*, 13, 10733-10753,
1341 <https://doi.org/10.5194/acp-13-10733-2013>, 2013b.



1342 Zhao, C., Hu, Z., Qian, Y., Leung, L. R., Huang, J., Huang, M., Jin, J., Flanner, M. G.,
1343 Zhang, R., Wang, H., Yan, H., Lu, Z., and Streets, D. G.: Simulating black carbon
1344 and dust and their radiative forcing in seasonal snow: a case study over North
1345 China with field campaign measurements, *Atmospheric Chemistry and Physics*, 14,
1346 11475-11491, <https://doi.org/10.5194/acp-14-11475-2014>, 2014.

1347 Zhao, C., Huang, M., Fast, J. D., Berg, L. K., Qian, Y., Guenther, A., Gu, D.,
1348 Shrivastava, M., Liu, Y., Walters, S., Pfister, G., Jin, J., Shilling, J. E., and Warneke,
1349 C.: Sensitivity of biogenic volatile organic compounds to land surface
1350 parameterizations and vegetation distributions in California, *Geoscientific Model
1351 Development*, 9, 1959-1976, <https://doi.org/10.5194/gmd-9-1959-2016>, 2016.

1352 Zheng, B., Tong, D., Li, M., Liu, F., Hong, C., Geng, G., Li, H., Li, X., Peng, L., Qi, J.,
1353 Yan, L., Zhang, Y., Zhao, H., Zheng, Y., He, K., and Zhang, Q.: Trends in China's
1354 anthropogenic emissions since 2010 as the consequence of clean air actions,
1355 *Atmospheric Chemistry and Physics*, 18, 14095-14111,
1356 <https://doi.org/10.5194/acp-18-14095-2018>, 2018.

1357
1358
1359
1360
1361
1362
1363
1364
1365
1366
1367
1368
1369
1370
1371

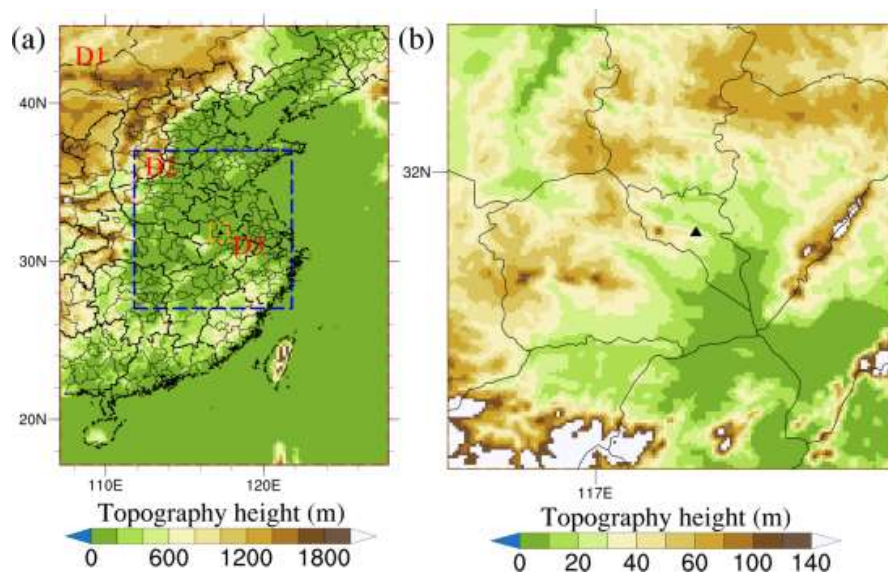


1372

Table 1 WRF-Chem model configuration

Horizontal resolution	25, 5, and 1 km
Domain size (grid cells)	140 × 105, 250 × 250, and 150 × 150
Simulation period	5 to 21 March 2019
Gas-phase chemistry scheme	CBMZ mechanism
Radiation scheme	Fast-J
PBL scheme	Yonsei University (YSU) scheme
Microphysics scheme	Morrison two-moment scheme
Land surface scheme	Noah land surface scheme
Cumulus scheme	Kain-Fritsch (25 km grid only)
Surface layer scheme	Revised MM5 Monin-Obukhov scheme
Longwave radiation scheme	RRTMG scheme
Shortwave radiation scheme	RRTMG scheme

1373
1374
1375
1376
1377
1378
1379
1380
1381
1382
1383
1384
1385
1386
1387
1388
1389
1390
1391
1392
1393
1394
1395
1396



1397

1398

1399

1400

1401

1402

1403

1404

1405

1406

1407

1408

1409

1410

1411

1412

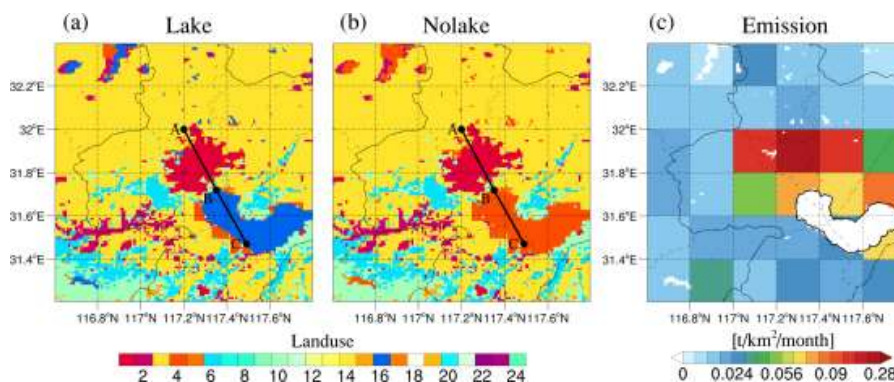
1413

1414

1415

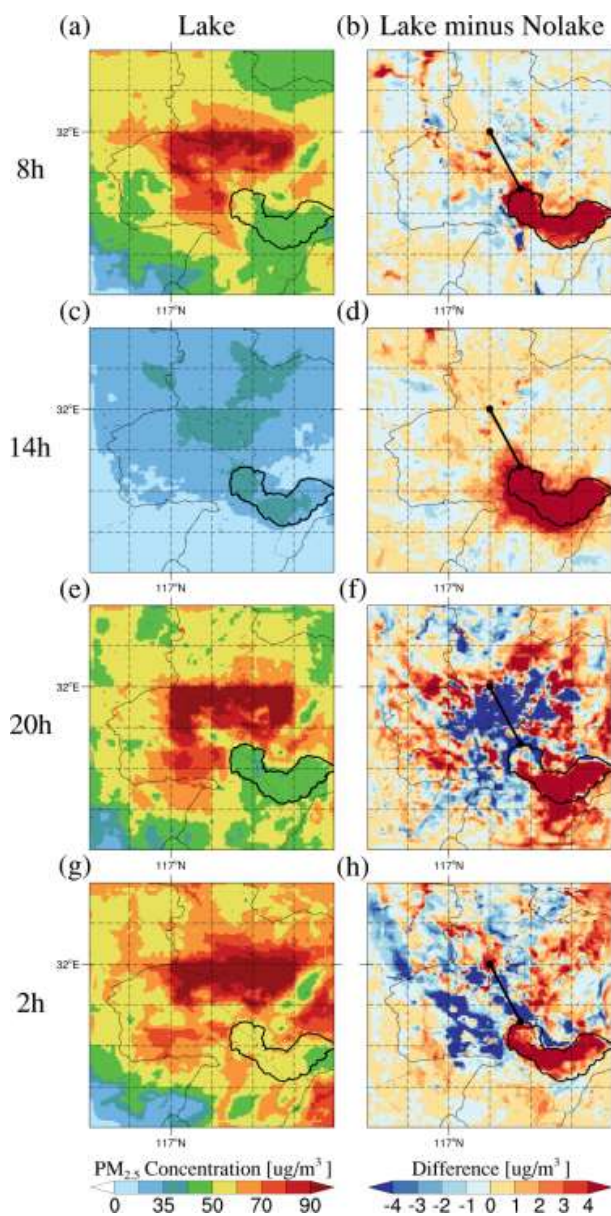
1416

Figure 1. (a) The three domains used in the WRF-Chem simulations and the terrain height (m) of each domain. Domain one (D1) has a horizontal grid spacing of 25 km, domain 2 (D2) 5 km, and domain 3 (D3) 1 km; (b) The spatial distribution of the terrain height (m) in D3. The solid black triangle indicates the location of Hefei.



1417
1418 **Figure 2.** The spatial distribution of land use types in the (a) Lake experiment and (b)
1419 Nolake experiment across the study area, with detailed descriptions of the legend and
1420 land cover classes provided in Table S1 in the Supplement. (c) The spatial distribution
1421 of PM_{2.5} emissions in both the Lake and Nolake experiments averaged over the entire
1422 day throughout the study area. The black line segments (AB and BC) in panels (a) and
1423 (b) represent transects selected for subsequent detailed analyses, traversing both urban
1424 and lake regions to capture the spatial characteristics of lake-urban interactions.

1425
1426
1427
1428
1429
1430
1431
1432
1433
1434
1435
1436
1437
1438
1439



1440

1441 **Figure 3.** The spatial distribution of PM_{2.5} surface concentrations in the (a, c, e, g)

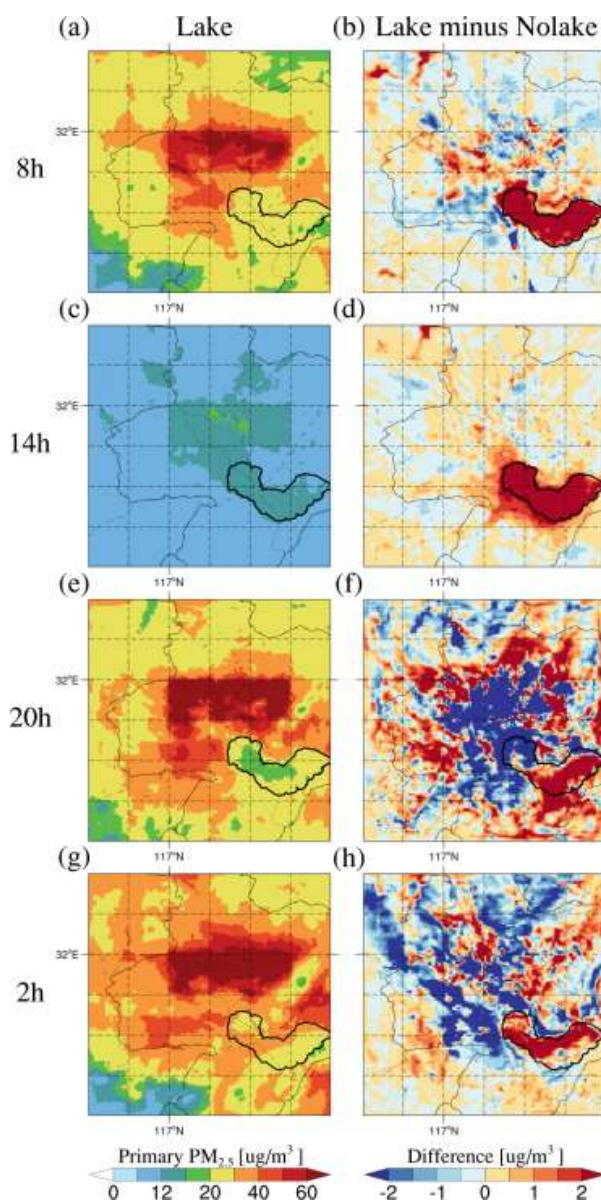
1442 Lake experiment and (b, d, f, h) the differences between Lake and Nolake experiments

1443 (Lake minus Nolake) at 08:00, 14:00, 20:00, and 02:00 local time (LT) across the study

1444 area. Note that the line segments shown in panels (b, d, f, h) correspond to the AB

1445 transect marked in Figure 2.

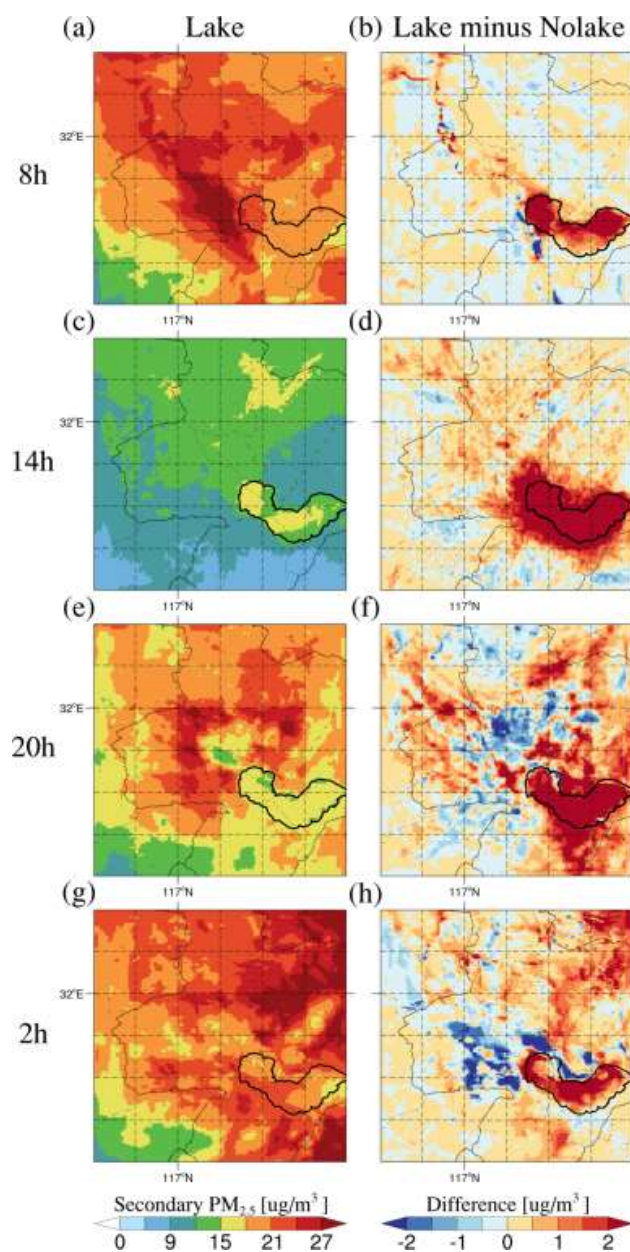
1446



1461

1462 **Figure 5.** The spatial distribution of primary $\text{PM}_{2.5}$ surface concentrations (sum of black
1463 carbon (BC), organic carbon (OC), and other inorganics (OIN)) in the (a, c, e, g) Lake
1464 experiment and (b, d, f, h) the differences between Lake and Nolake experiments
1465 (Lake minus Nolake) at 08:00, 14:00, 20:00, and 02:00 LT across the study area.

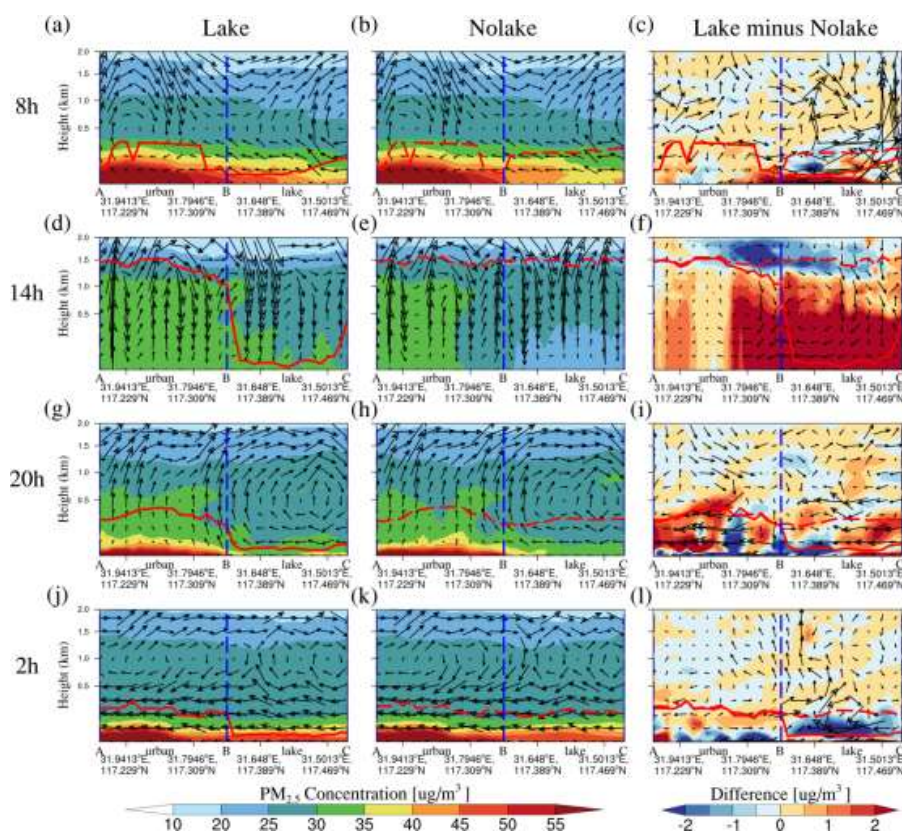
1466



1467

1468 **Figure 6.** The spatial distribution of secondary PM_{2.5} surface concentrations (sum of
1469 sulfate (SO_4^{2-}), nitrate (NO_3^-), and ammonium (NH_4^+)) in the (a, c, e, g) Lake
1470 experiment and (b, d, f, h) the differences between Lake and Nolake experiments
1471 (Lake minus Nolake) at 08:00, 14:00, 20:00, and 02:00 LT across the study area.

1472



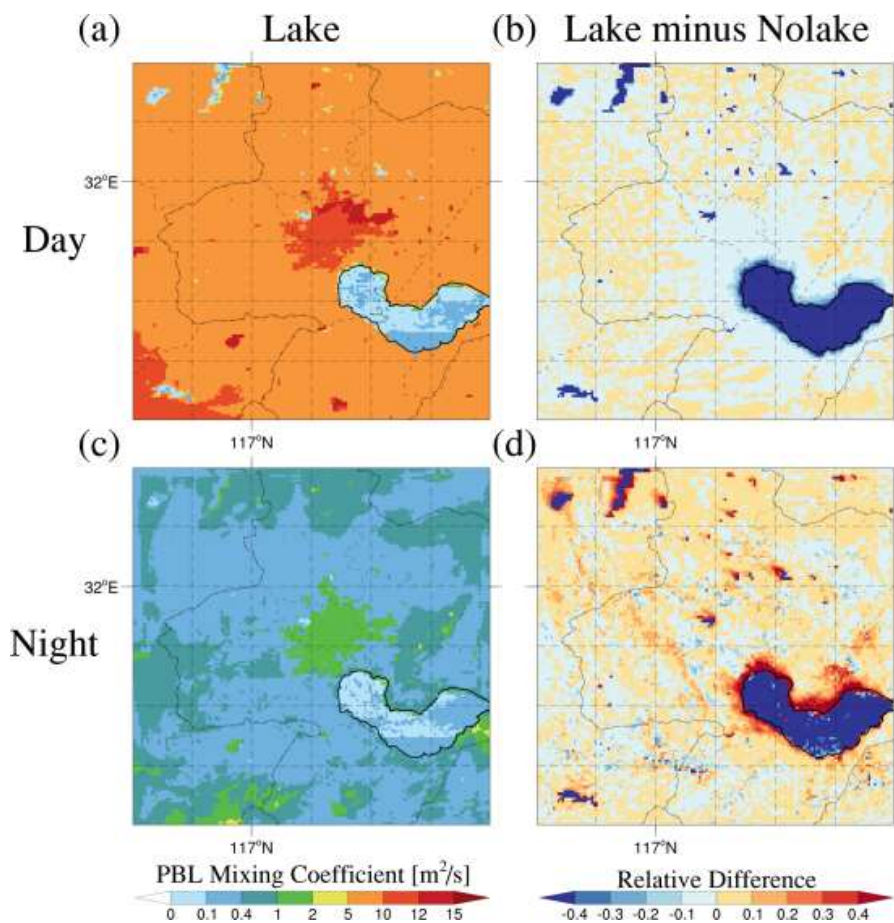
1473

1474 **Figure 7.** The vertical cross-section of PM_{2.5} concentration and wind speed along the
 1475 key path AC (indicated in Figure 2) for the (a, d, g, j) Lake experiment, (b, e, h,
 1476 k) Nolake experiment, and (c, f, i, l) their differences (Lake minus Nolake) at 08:00,
 1477 14:00, 20:00, and 02:00 LT. The shaded contours represent PM_{2.5} concentrations or their
 1478 differences between the two experiments at each altitude. The black vector arrows
 1479 indicate the superimposed vertical wind field (including horizontal and vertical wind
 1480 components), with the vertical wind speed being multiplied by 50 for visibility. The red
 1481 solid line represents the planetary boundary layer height (PBLH) in the Lake
 1482 experiment, and the red dashed line represents the planetary boundary layer height in
 1483 the Nolake experiment. The blue dashed line represents the lake-land boundary.

1484

1485

1486



1487

1488 **Figure 8.** The spatial distribution of planetary boundary layer (PBL) mixing
1489 coefficients averaged during (a, b) daytime (08:00, 11:00, 14:00, and 17:00 LT) and (c,
1490 d) nighttime (20:00, 23:00, 02:00, and 05:00 LT) for the (a, c) Lake experiment and (b,
1491 d) relative differences ((Lake - Nolake)/Lake) across the study area.

1492

1493

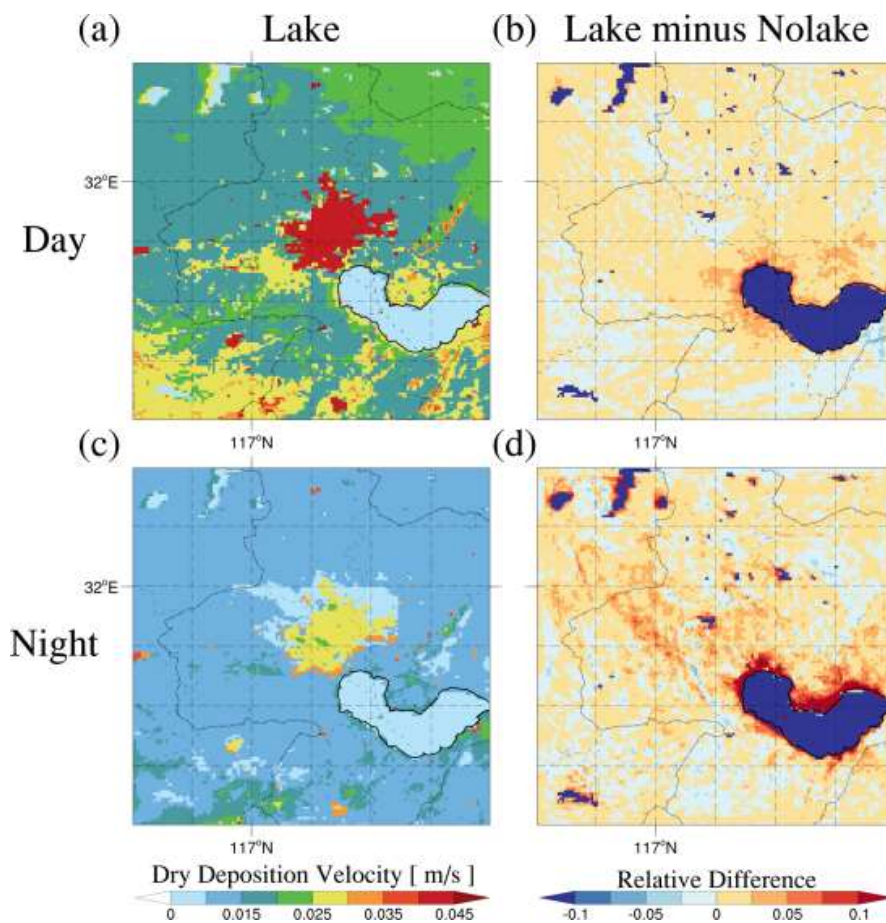
1494

1495

1496

1497

1498



1499

1500 **Figure 9.** The spatial distribution of dry deposition velocity averaged during (a, b)
1501 daytime (08:00, 11:00, 14:00, and 17:00 LT) and (c, d) nighttime (20:00, 23:00, 02:00,
1502 and 05:00 LT) for the (a, c) Lake experiment and (b, d) relative differences ((Lake -
1503 Nolake)/Lake) across the study area.

1504

1505

1506

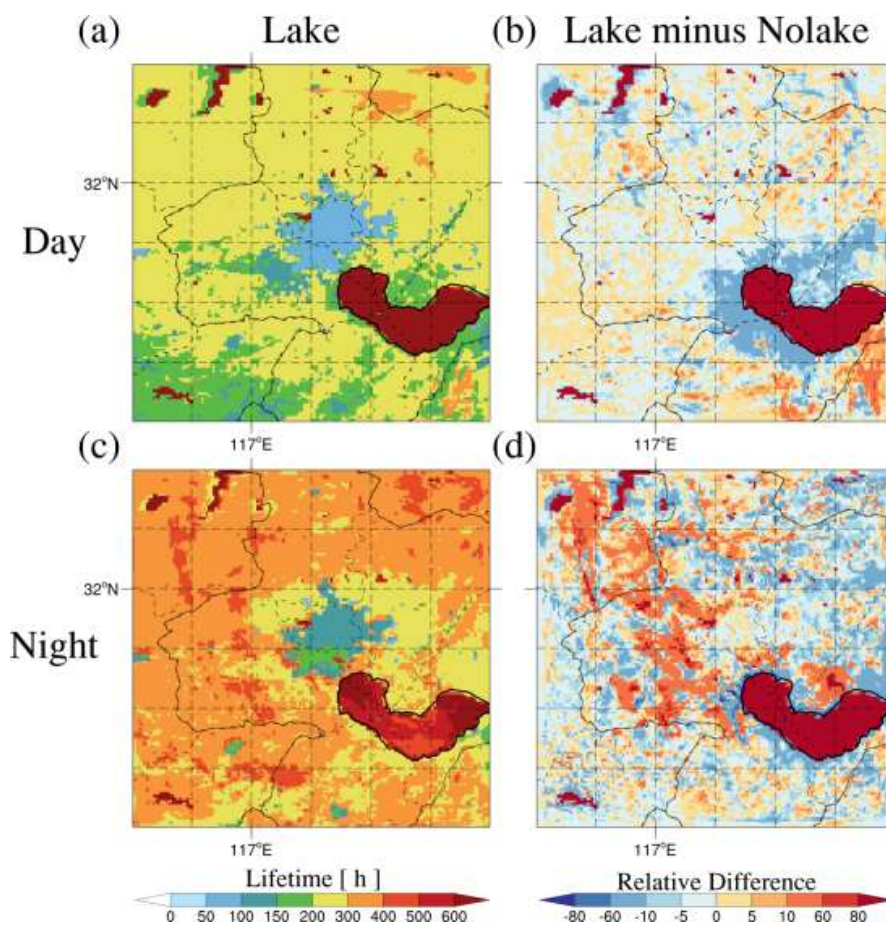
1507

1508

1509

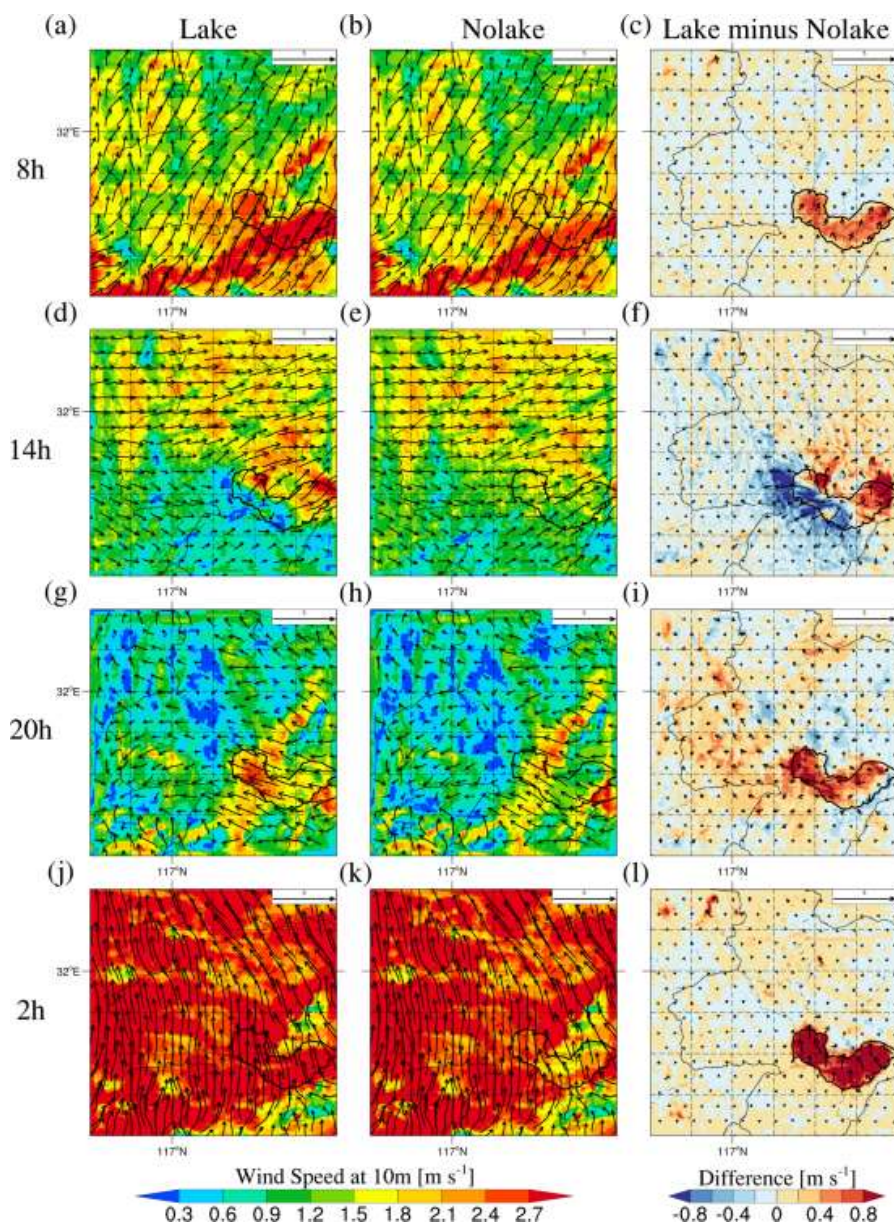
1510

1511



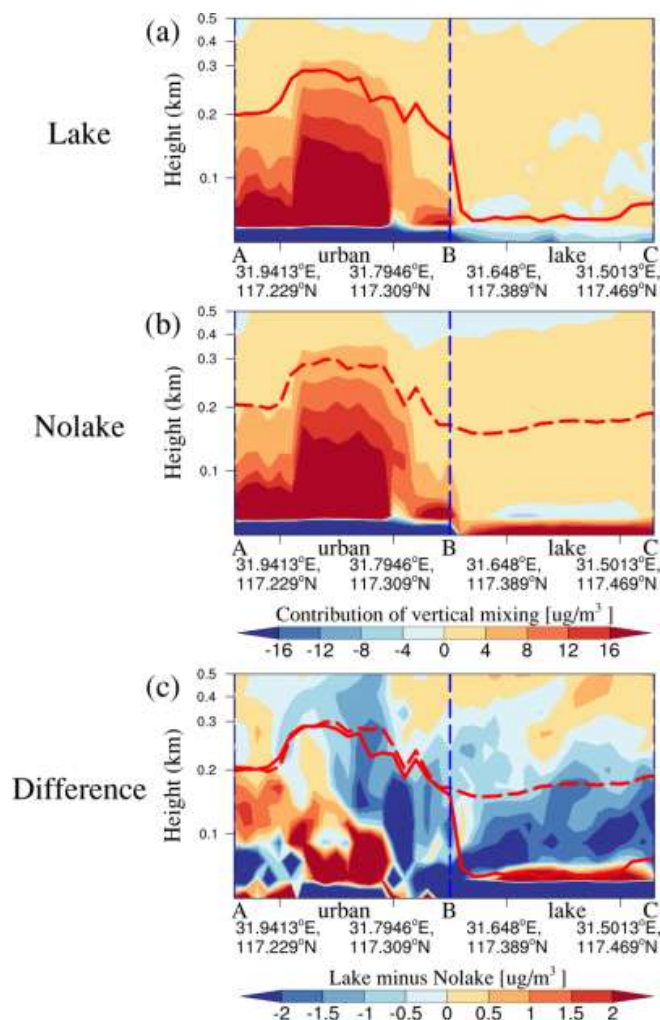
1512
1513 **Figure 10.** The spatial distribution of the lifetime averaged during (a, b) daytime (08:00,
1514 11:00, 14:00, and 17:00 LT) and (c, d) nighttime (20:00, 23:00, 02:00, and 05:00 LT)
1515 for the (a, c) Lake experiment and (b, d) relative differences $((\text{Lake} - \text{Nolake})/\text{Lake})$
1516 across the study area. The $\text{PM}_{2.5}$ lifetime is calculated by dividing the $\text{PM}_{2.5}$ column
1517 concentration by the dry deposition flux.

1518
1519
1520
1521
1522
1523
1524

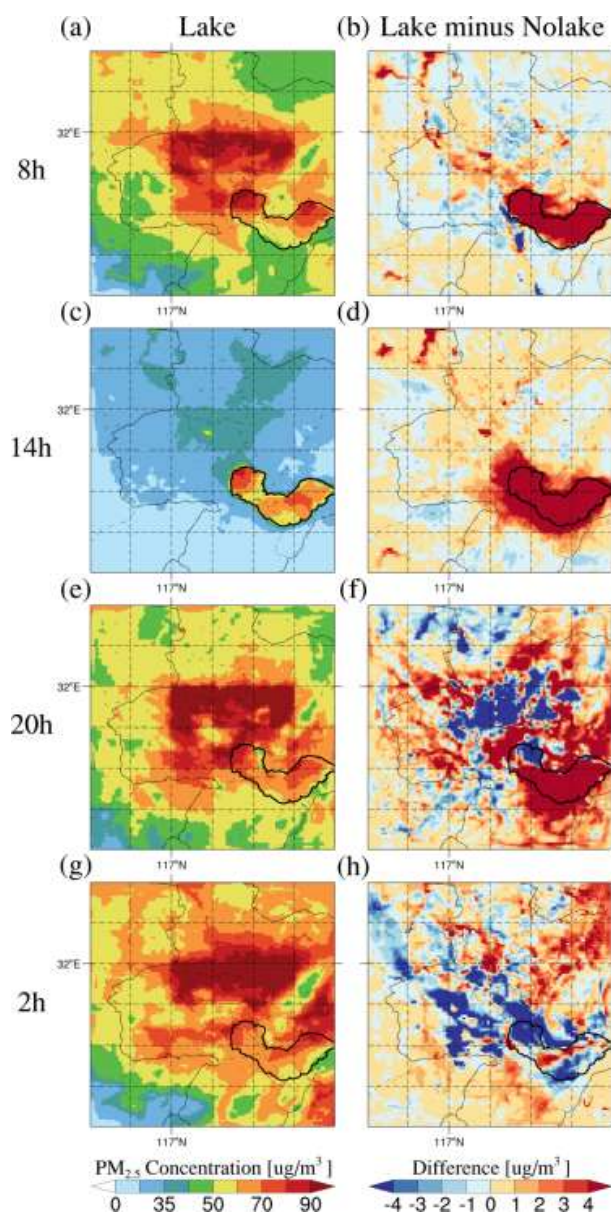


1525
1526 **Figure 11.** The spatial distribution of 10-m wind speed in the (a, d, g, j) Lake
1527 experiment, (b, e, h, k) Nolake experiment, and (c, f, i, l) their differences (Lake
1528 minus Nolake) at 08:00, 14:00, 20:00, and 02:00 LT across the study area. Note that the
1529 line segments in Figures 3c, f, i, and l correspond to the BA line segment in Figure 2.

1530
1531



1532
1533 **Figure 12.** The vertical cross-section of PBL mixing process contributions to $PM_{2.5}$
1534 concentrations along the key path AC (indicated in Figure 2) for the (a) Lake
1535 experiment, (b) Nolake experiment, and (c) their differences (Lake minus Nolake)
1536 averaged at nighttime. The shaded contours represent the contribution of PBL mixing
1537 processes to surface $PM_{2.5}$ concentrations or their differences between the two
1538 experiments at each altitude. The red solid line represents the PBLH in the Lake
1539 experiment, and the red dashed line represents the PBLH in the Nolake experiment. The
1540 blue dashed line represents the lake-land boundary.
1541



1542

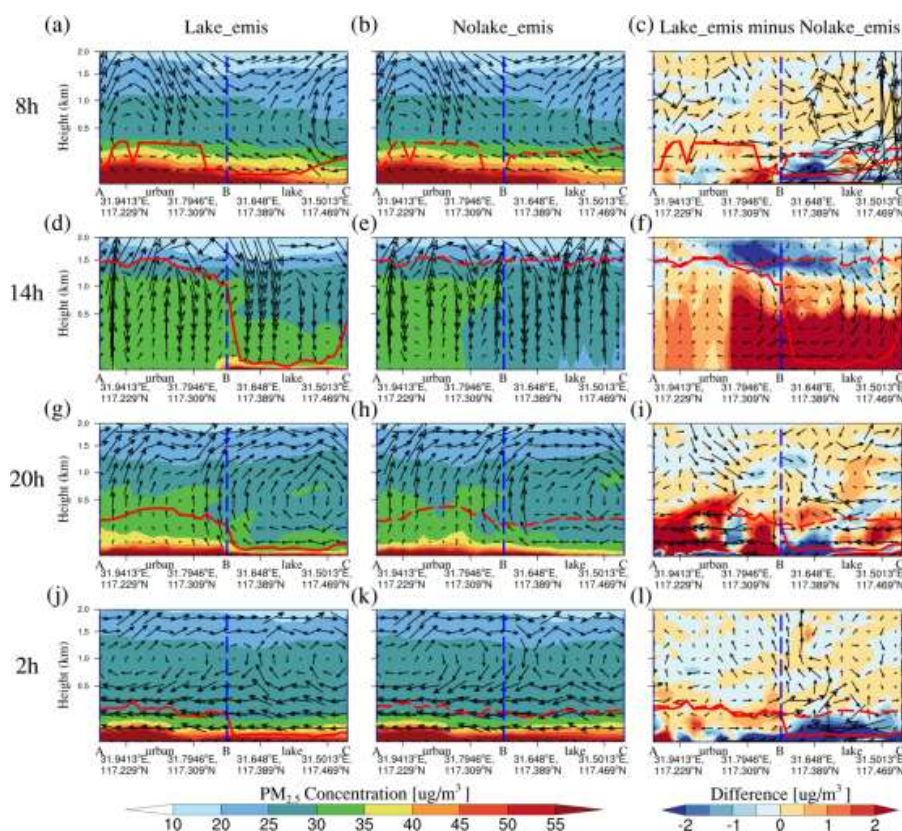
1543 **Figure 13.** The spatial distribution of PM_{2.5} surface concentrations in the (a、c、e、g)

1544 Lake_emis experiment and (b、d、f、h) the differences between Lake_emis and

1545 Nolake_emis experiments (Lake_emis minus Nolake_emis) at 08:00, 14:00, 20:00, and

1546 02:00 LT across the study area.

1547



1548

1549 **Figure 14.** The vertical cross-section of $PM_{2.5}$ concentration and wind speed along the
 1550 key path AC (indicated in Figure 2) for the (a, d, g, j) Lake_emis experiment, (b,
 1551 e, h, k) Nolake_emis experiment, and (c, f, i, l) their differences (Lake_emis minus
 1552 Nolake_emis) at 08:00, 14:00, 20:00, and 02:00 LT. The shaded contours represent
 1553 $PM_{2.5}$ concentrations or their differences between the two experiments at each altitude.
 1554 The black vector arrows indicate the superimposed vertical wind field (including
 1555 horizontal and vertical wind components), with the vertical wind speed being multiplied
 1556 by 50 for visibility. The red solid line represents the planetary boundary layer height
 1557 (PBLH) in the Lake experiment, and the red dashed line represents the planetary
 1558 boundary layer height in the Nolake experiment. The blue dashed line represents the
 1559 lake-land boundary.

1560

1561